Cell Reports
Medicine

Article

Personalized drug screening using patient-derived organoid and its clinical relevance in gastric cancer

Graphical abstract

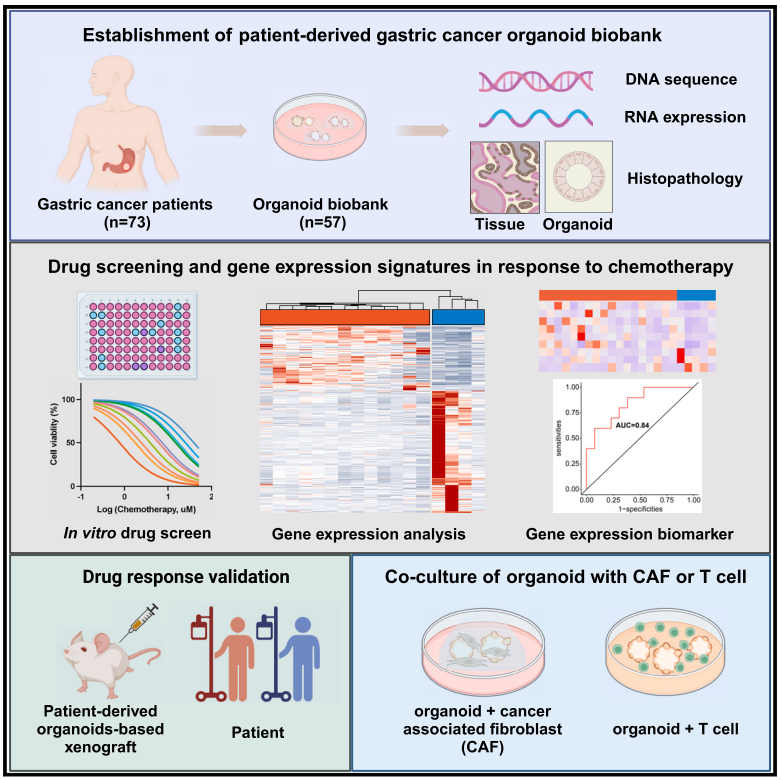

Highlights

- Establishment of a biobank comprising living gastric cancer (GC) organoids
- Identification of a chemosensitivity-associated gene expression signature
- GC organoids reproduce chemotherapeutic drug responses of patients *in vitro* and *in vivo*
- GC organoids can be co-cultured with T cells and cancer-associated fibroblasts

Authors

Yi Zhao, Shangru Li, Lefan Zhu, ..., Lixia Xu, Jun Yu, Xiaoxing Li

Correspondence

xulixia@mail.sysu.edu.cn (L.X.), junyu@cuhk.edu.hk (J.Y.), lixiaox23@mail.sysu.edu.cn (X.L.)

In brief

Yi et al. present the establishment of a biobank of gastric cancer organoids derived from patients. These organoids mirror the complex dynamics of chemotherapy response. It may offer a valuable tool for the refinement of personalized treatments and the prediction of individual patient responses to chemotherapy.

Zhao et al., 2024, Cell Reports Medicine *5*, 101627
July 16, 2024
https://doi.org/10.1016/j.xcrm.2024.101627

CellPress

Cell Reports Medicine

CellPress
OPEN ACCESS

Article

Personalized drug screening using patient-derived organoid and its clinical relevance in gastric cancer

Yi Zhao,[1,2,6] Shangru Li,[1,6] Lefan Zhu,[2,6] Mingle Huang,[1] Yubin Xie,[2] Xinming Song,[3] Zhihui Chen,[3] Harry Cheuk-Hay Lau,[4] Joseph Jao-Yiu Sung,[2,5] Lixia Xu,[1,2,*] Jun Yu,[2,4,*] and Xiaoxing Li[2,7,*]

[1]Department of Oncology, The First Affiliated Hospital, Sun Yat-sen University, Guangzhou, China
[2]Institute of Precision Medicine, The First Affiliated Hospital, Sun Yat-sen University, Guangzhou, China
[3]Department of Gastrointestinal Surgery, The First Affiliated Hospital, Sun Yat-sen University, Guangzhou, China
[4]Department of Medicine and Therapeutics, State Key Laboratory of Digestive Disease, The Chinese University of Hong Kong, Hong Kong SAR, China
[5]Lee Kong Chian School of Medicine, Nanyang Technological University, Singapore, Singapore
[6]These authors contributed equally
[7]Lead contact
*Correspondence: xulixia@mail.sysu.edu.cn (L.X.), junyu@cuhk.edu.hk (J.Y.), lixiaox23@mail.sysu.edu.cn (X.L.)
https://doi.org/10.1016/j.xcrm.2024.101627

SUMMARY

The efficacy of chemotherapy varies significantly among patients with gastric cancer (GC), and there is currently no effective strategy to predict chemotherapeutic outcomes. In this study, we successfully establish 57 GC patient-derived organoids (PDOs) from 73 patients with GC (78%). These organoids retain histological characteristics of their corresponding primary GC tissues. GC PDOs show varied responses to different chemotherapeutics. Through RNA sequencing, the upregulation of tumor suppression genes/pathways is identified in 5-fluorouracil (FU)- or oxaliplatin-sensitive organoids, whereas genes/pathways associated with proliferation and invasion are enriched in chemotherapy-resistant organoids. Gene expression biomarker panels, which could distinguish sensitive and resistant patients to 5-FU and oxaliplatin (area under the dose-response curve [AUC] >0.8), are identified. Moreover, the drug-response results in PDOs are validated in patient-derived organoids-based xenograft (PDOX) mice and are consistent with the actual clinical response in 91.7% (11/12) of patients with GC. Assessing chemosensitivity in PDOs can be utilized as a valuable tool for screening chemotherapeutic drugs in patients with GC.

INTRODUCTION

Gastric cancer (GC) is the fifth most common cancer and the fourth most common cause of cancer death globally, and its incidence rate has increased over the last decades.[1] Surgical resection combined with perioperative chemotherapy is the first-line curative option for patients with locally advanced GC.[2] The most common conventional chemotherapeutic drugs include fluorouracil (e.g., 5-fluorouracil [5-FU], capecitabine, and S-1) and platinum compounds (e.g., cisplatin and oxaliplatin).[3–5] However, the responses of patients with GC to these chemotherapies are highly varied without clear reasons.[6,7] To improve the efficacy of chemotherapy and clinical outcome, it is therefore unmet to develop approaches that can accurately predict the efficacy of chemotherapy in patients with GC.

Organoid cultures are three-dimensional cell aggregates. Recent studies have reported that patient-derived organoids (PDOs) can be predictive of patient's treatment response.[8,9] In particular, PDOs could accurately preserve and recapitulate both the genetic landscape and histopathological features of their originated tumors, implicating their potential application in personalized cancer treatment.[10] Three independent groups reported the establishment of PDOs derived from patients with GC and explored the application of PDOs for predicting drug responses.[11–13] However, these studies lack investigation into gene expression characteristics related to chemosensitivity. Gene signatures characterized from organoids or original tumor tissues can facilitate the identification of predictive biomarkers of treatment response[14,15]; hence, integrated analyses on gene expression and chemosensitivity based on PDOs are therefore important. Moreover, the sample sizes of previous studies of drug screening on GC PDOs were relatively small.[11–13] Performing drug screening on a large collection of GC PDOs is necessary to provide accurate and reliable personalized treatment prediction for patients with GC. Here, we reported the establishment of a patient-derived GC organoid biobank and their ability to model the histological features of human GC, as well as their responses to chemotherapeutic drugs. We analyzed the molecular characteristics of GC PDOs to identify marker genes associated with chemotherapeutic drug sensitivity and resistance. We also utilized a patient-derived organoids-based xenograft (PDOX) model to verify the results of drug sensitivity test from PDOs, and we further testified with actual treatment response in individual patients with GC.

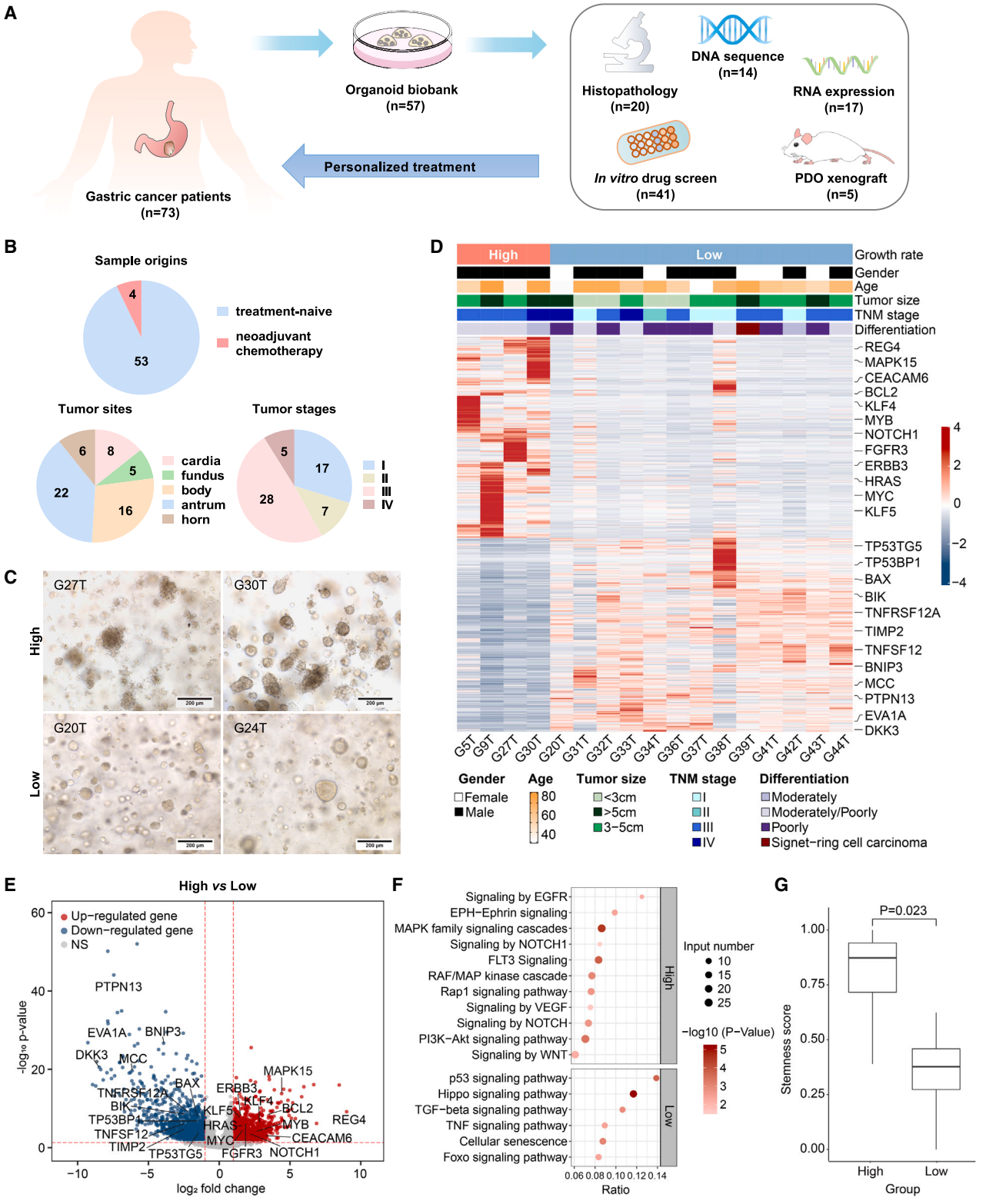

Figure 1. Establishing a living patient-derived GC organoid biobank

(A) Schematic of GC organoid culture establishment and analysis performed.

(B) Pie chart showing the sample origins, tumor sites, and TNM stages of the established 57 GC organoids.

(legend continued on next page)

RESULTS

Establishing a living patient-derived GC organoid biobank

We obtained gastric tumor tissues from 73 patients with histologically diagnosed gastric adenocarcinoma from surgical resection specimens. The clinicopathological characteristics of all patients are shown in Table S1. We successfully established 57 organoids derived from these GC tumor tissues with an overall success rate of 78% (57/73) (Figure 1A). Specifically, 53 organoids were derived from treatment-naive patients, and four organoids were derived from patients with neoadjuvant chemotherapy (Figure 1B). GC organoids were derived from various sites of the stomach, such as the cardia (n = 8), fundus (n = 5), body (n = 16), antrum (n = 22), and horn (n = 6). These organoids were obtained from patients with different tumor-node-metastasis (TNM) stages, including stage I (n = 17), II (n = 7), III (n = 28), and IV (n = 5) (Figure 1B).

Distinct GC organoids had different growth rates. Five organoid cultures could be serially propagated for up to 17 passages without any apparent diminution in their ability to propagate. These organoids including G5T, G9T, G27T, G30T, and G72T were therefore defined as high-growth-rate organoids, which showed a proliferative progenitor phenotype and the formation of a spheroid, cyst-like morphology without lumen (Figure 1C). Other organoid cultures were successfully established but failed to further propagate after 8–9 passages; hence, they were defined as low-growth-rate organoids. These 52 low-growth-rate organoids had a glandular morphology with the appearance of lumens (Figure 1C). Thus, these results indicated that we have successfully established a biobank of GC PDOs. These organoids had different growth features, such as high-growth-rate or low-growth-rate organoids.

Elucidating gene expression profiles in organoids with high growth rate or low growth rate

RNA sequencing was conducted to compare GC organoids with high growth rate or low growth rate. The significant differential gene expression was identified in high-growth-rate organoids compared to low-growth-rate organoids (Figure 1D). Proliferation- and stemness-related genes *REG4*, *KLF4*, *ERBB3*, *HRAS*, *NOTCH1*, and *MYC* were outlier genes and significantly upregulated in high-growth-rate organoids (Figure 1E), while genes related to cell growth inhibition, including *BAX*, *DKK3*, *TNFSF12*, *MCC*, *BNIP3*, and *TP53BP1*, were downregulated in high-growth-rate organoids compared to low-growth-rate organoids (Figures 1D and 1E). Consistently, Kyoto Encyclopedia of Genes and Genomes (KEGG) Orthology-Based Annotation System (KOBAS) of differentially expressed genes confirmed that proliferation- and stemness-related pathways were more upregulated in high-growth-rate organoids, including mitogen-activated protein kinase (MAPK) family signaling cascades and signaling by NOTCH, all of which could accelerate cell proliferation and maintain stem function (Figure 1F). Cell differentiation and apoptosis-related pathways, including the Hippo signaling pathway and the p53 signaling pathway, were relatively downregulated in high-growth-rate organoids compared to low-growth-rate organoids (Figure 1F). The high-growth-rate organoids also had higher stemness score (0.784) in comparison to low-growth-rate organoids (0.345) ($p < 0.05$) (Figure 1G). Additionally, we analyzed the correlation between the growth rates of organoids and clinic pathological parameters and found that the growth rates (high growth rate vs. low growth rate) of organoids did not exhibit a significant correlation with clinicopathologic characteristics (Table S2). Whole-exome sequencing was conducted to examine the mutational profiles of organoids in terms of growth rate. There was no significant difference for gene mutations between high-growth-rate organoids and low-growth-rate organoids, including the well-known driver mutations of *TP53*, *CDH1*, *ARID1A*, *MUC6*, and *RNF43* (Figure S1). Hence, high-growth organoids and low-growth organoids have different gene expression patterns. High-growth organoids showed more robust proliferation and stemness properties, which could at least in part explain their difference in growth features.

Gene expression analysis of GC organoids and corresponding tumor tissue

Next, we investigated how stable tumor-specific gene expression is maintained in organoid culture. We have now compared the RNA sequencing results of organoids and primary tumors. We observed a high degree of similarity in gene expression patterns between organoids and their corresponding primary tumor tissues by RNA sequencing (Figures 2A and 2B). To test the similarity between primary tumors and organoids, we quantitatively analyzed and compared gene expression at the level of alternative transcripts from RNA sequencing (in $\log_2$ fragments per kilobase of exon model per million mapped fragments) in primary tumors and organoids. A high level of concordance in gene expression was demonstrated between the matched organoids and primary tumors (average ρ: 0.785, average R^2:0.64) (Figure S2A).

GC organoids preserve the histopathologic characteristics of their derived primary GCs

We assessed whether GC organoids could preserve the histological characteristics and protein expression of their originated tumors. As expected, GC organoids retained specific glandular features that were observed in their corresponding primary tumors, including glandular, discohesive, or solid growth pattern and nuclear stratification (Figures 2C and S2B). The organoids also exhibited similar histological features as the subtypes of their corresponding primary tumors including diffuse type,

(C) Representative pictures of 2 GC organoids with high growth rate and 2 with low growth rate. Scale bar, 200 μm.
(D and E) Heatmap and volcano plot analysis showing the most significantly differential genes in GC organoids with high growth rate (n = 4) compared to organoids with low growth rate (n = 13). The colored bar represents the log2-transformed values. Individual genes are denoted by gene name. Differentially expressed genes ($p < 0.05$, log2 (fold change) > 1) of high-growth-rate organoids and low-growth-rate organoids are indicated in red or blue, respectively.
(F) KOBAS of the differential gene expression profiles of high-growth-rate organoids compared to the low-growth-rate organoids.
(G) Stemness score analysis between high-growth-rate organoids and low-growth-rate organoids.

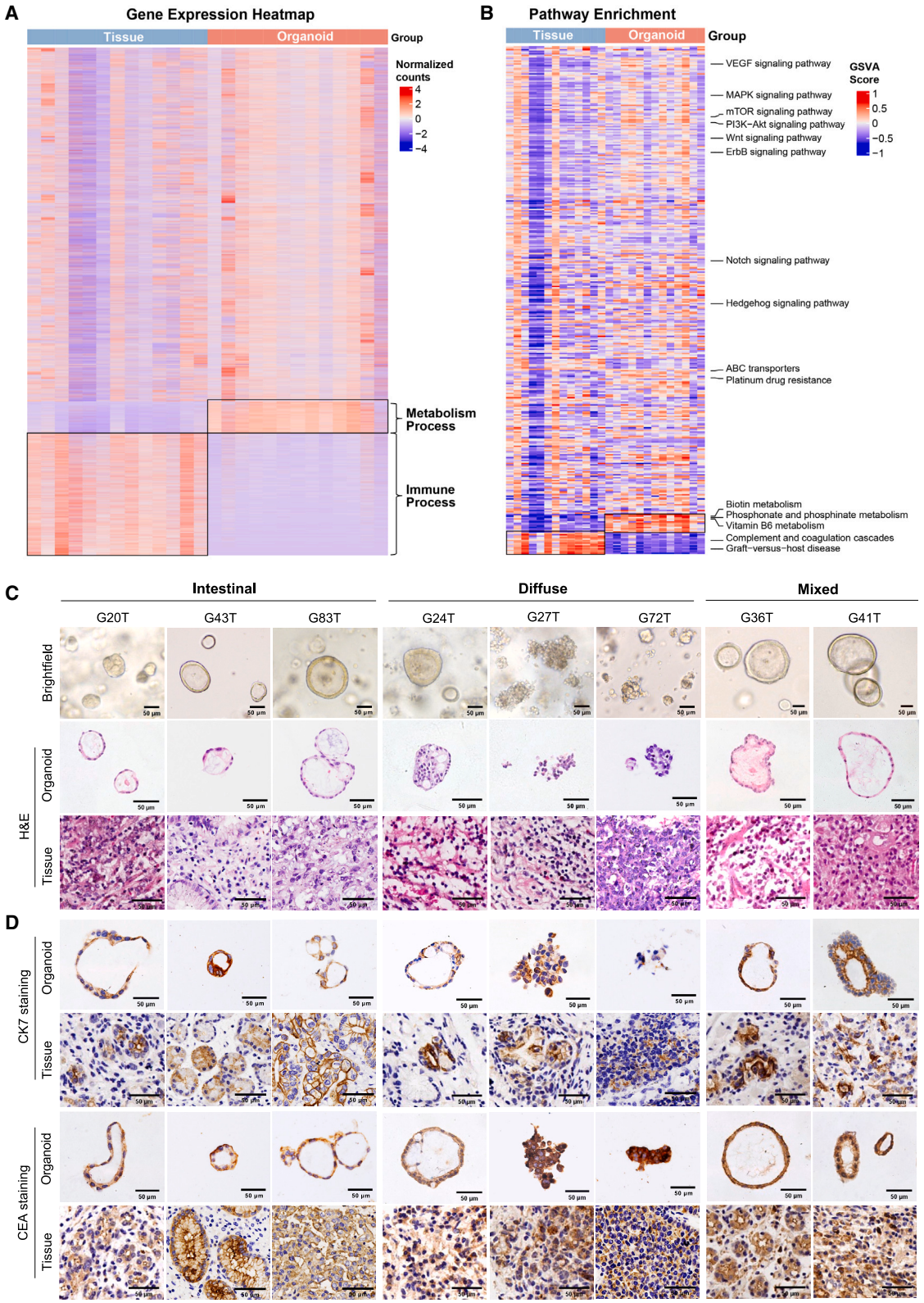

(legend on next page)

intestinal type, and mixed type of GC. GC organoids derived from intestinal-type tumors (G20T and G43T) exhibited a large sphere that consisted of a single epithelial layer or cribriform glandular morphology with cells forming multiple lumens of varying sizes. GC organoids derived from diffuse-type tumors (G27T and G72T) formed loosely cohesive solid cell clusters, or cystic structures (G24T and G39T). GC organoid derived from mixed-type GC (G36T and G41T) displayed either or both histological patterns of diffuse- and intestinal-type tumors (Figures 2C and S2B). To confirm that GC organoids maintained the characteristics of their originated tumors, we performed immunohistochemistry for the protein expression of GC markers cytokeratin 7 (CK7) and carcinoembryonal antigen (CEA). As shown in Figures 2D and S2C, GC organoids displayed a similar presence and intensity of these protein markers compared to their corresponding primary tumors. We found that the Allred scores of CK7 and CEA intensity from the organoid line and the original tumors were highly correlated (Pearson correlation R^2 is 0.87 and 0.91, respectively) (Figure S2D). Due to the heterogeneity of the tumor tissue, we also checked the inconsistent cases and found that the expression intensity of CK7 (in G43T and G56T) and CEA (in G62T and G56T) was different between the original tumors and organoids (Figure S2D). These results indicated that GC organoids retained the histopathologic features of their primary tumors, inferring that GC PDOs could mimic primary GCs of individual patients for drug testing.

Drug screening of GC PDOs to chemotherapeutics

To explore the responses of GC organoids to different drugs, six conventional chemotherapeutics were applied to 41 GC organoids. Each drug was screened at five different concentrations in triplicate. Specifically, according to previous studies,[11] GC organoids were exposed to different fixed concentrations of 5-FU (0.2, 1, 5, 10, and 50 μmol/L), oxaliplatin (0.2, 1, 5, 10, and 50 μmol/L), cisplatin (0.2, 1, 5, 10, and 50 μmol/L), paclitaxel (0.01, 0.1, 1, 10, and 100 nmol/L), doxorubicin (0.0001, 0.001, 0.01, 0.1, and 1 μmol/L), or SN-38 (0.01, 0.1, 1, 10, and 100 nmol/L), respectively. Two different passages of each organoid line were treated with the aforementioned drugs in different concentrations to evaluate their responses. We found that the area under the dose-response curve (AUC) values of biological replicates from two organoid passages of the same organoid line were highly correlated (Pearson correlation $R^2 > 0.87$), indicating that our culture system is stable and unaffected by external conditions and the disparity in organoid passages (Figures 3A and S3A). To ensure the accuracy of half-maximal inhibitory concentration (IC50) estimates, we tested the sensitivity of the drugs using an additional ten-concentration system. Our analysis revealed a strong correlation between the AUC values and IC50 values obtained from two sets of drug concentrations (ten concentrations and five concentrations) derived from the same organoid line (Pearson correlation $R^2 > 0.92$) (Figures S3B and S3C). We observed that the responses to chemotherapeutic drugs varied among organoids generated from different patients with GC (Figure 3B; Table S3). Some organoids were resistant, and some others were partially sensitive or sensitive to 5-FU, oxaliplatin, cisplatin, paclitaxel, SN-38, and doxorubicin (Figure 3C). The organoids generated from diffuse-type GC were more likely to be sensitive to 5-FU and paclitaxel (Figure 3C). These results collectively suggested that GC PDOs are potentially effective tools for drug screening with varied responses to different conventional chemotherapeutics.

Gene expression signatures of GC PDOs in response to chemotherapeutics

We analyzed the gene expression signatures of 17 PDOs by transcriptional sequencing according to their responses to 5-FU or oxaliplatin, the most conventional chemotherapeutic drugs for patients with GC. The 17 GC organoids were separated into either sensitive or resistance groups based on their responses to 5-FU or oxaliplatin (sensitive: AUC <50%, resistance: AUC ≥50%). The gene expression profiles were compared between sensitive or resistant groups, and differential gene expression was demonstrated in GC organoids of the sensitive (n = 13) and resistance groups (n = 4) to 5-FU (Figure 4A). Significantly upregulated tumor suppression genes were identified in the 5-FU-sensitive group compared to 5-FU-resistant organoids, including *MSMB*, *S1PR4*, *PURPL*, *TP53INP1*, and *TRIM16* (Figure 4B). KOBAS demonstrated the upregulation of the tumor-suppressing p53 signaling pathway and cellular senescence in 5-FU-sensitive organoids (Figure 4C), while genes associated with proliferation and invasion, such as *FKBP10*, *DARPP32*, *ASCL2*, *BCL2*, *ABCC2*, and *NOTCH1*, were significantly downregulated in 5-FU-sensitive organoids compared to the resistant organoids (Figures 4A and 4B). These downregulated genes were enriched in tumor invasion and stemness-related pathways including NOTCH signaling, WNT signaling, Rho GTPases signaling, and extracellular matrix organization (Figure 4C).

Differential gene expression was also observed in GC organoids of sensitive (n = 11) and resistant groups (n = 6) to oxaliplatin (Figure 4D). Genes related to tumor suppression were significantly upregulated in the oxaliplatin-sensitive group as compared to oxaliplatin-resistant organoids, including *MYO1A*, *CLDN3*, *DMBT1*, *TNFRSF1B*, and *TRIM15* (Figure 4E). These upregulated genes in oxaliplatin-sensitive organoids were mainly enriched in tumor-suppressing pathways particularly tumor necrosis factor (TNF) signaling and FOXO signaling (Figure 4F), while genes associated with proliferation and invasion were significantly downregulated in the oxaliplatin-sensitive group compared to the resistant group, including *NDUFA4L2*, *DKK4*, *KLK10*, *FOSL1*, *STC2*, and *L1CAM* (Figure 4E). These downregulated genes were involved in proliferative pathways including PI3K signaling and WNT signaling (Figure 4F). Collectively, we demonstrated the gene expression signatures of GC PDOs

Figure 2. Transcriptome analysis and histopathologic characteristics between GC organoids and their derived primary GCs

(A) Heatmap of differentially expressed genes and (B) pathways between organoids and their corresponding tumor tissue. The colored bar represents the log2-transformed values. Differentially expressed genes ($p < 0.05$, log2 (fold change) > 1) of organoids and tissue are indicated in red or blue, respectively.

(C) Representative images of bright-field microscopy, hematoxylin and eosin staining of GC organoids, and matched primary GC tumor tissues.

(D) Immunohistochemistry of GC protein markers CK7 and CEA in organoids and their corresponding primary GC tumor tissues. Scale bar, 50 μm.

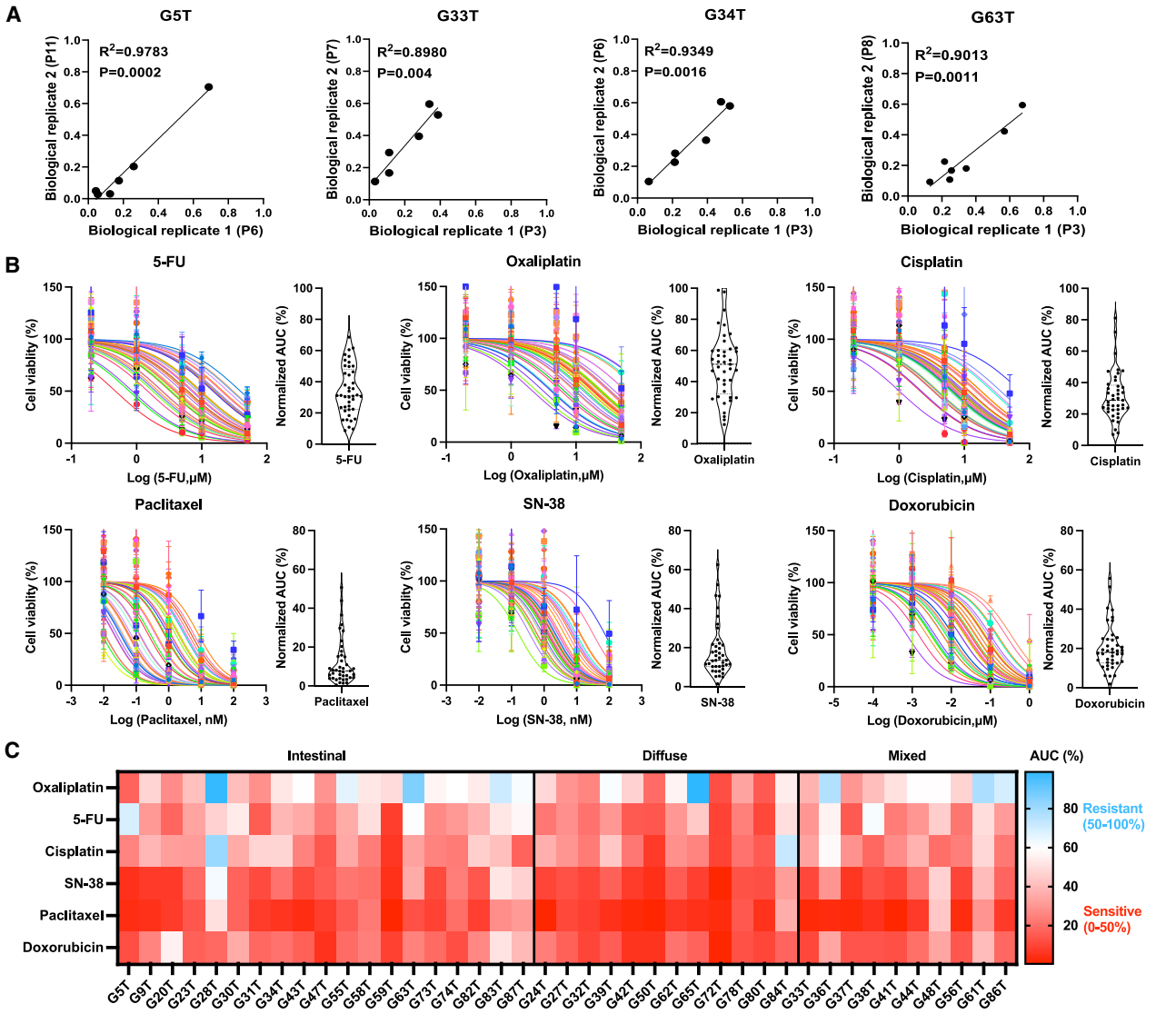

Figure 3. Drug screening of GC PDOs to chemotherapeutics

(A) Scatterplot showing the correlation between the 1-AUC values in two independent runs of drug screening ($n = 3$). Correlation is indicated as Pearson R^2 value.

(B) Dose-response curves showing the chemosensitivity of 41 GC organoids to 6 conventional chemotherapeutics (5-FU, oxaliplatin, cisplatin, paclitaxel, SN-38, and doxorubicin) ($n = 3$). AUC from dose-response data is displayed as a violin plot; every point indicates 41 GC organoids, respectively.

(C) Heatmap of AUC of 6 chemotherapeutics in 41 GC organoids. For each chemotherapeutic agent, the PDO library was divided into 2 subgroups: resistant (AUC = 50%–100%) and sensitive (AUC = 0%–50%).

in response to chemotherapeutics. Besides, we conducted functional experiments in organoids with knocked-out resistance or sensitivity genes identified by RNA sequencing. *MSMB* or *S1PR4* (5-FU-sensitive gene) knockout in G27T and G72T organoids significantly decreased drug sensitivity to 5-FU treatment compared with control cells (Figure 4G). Knockout of *FKBP10* (5-FU-resistant gene) in G9T organoids increased drug sensitivity to 5-FU treatment (Figure 4H). Knockout of *MYO1A* (oxaliplatin-sensitive gene) or *NDUFA4L2* (oxaliplatin-resistant gene) also decreased or increased drug sensitivity to oxaliplatin treatment (Figures 4I and 4J), respectively. These results confirmed the functional impact of these genes in organoids on their responses to 5-FU and oxaliplatin treatment.

Gene mutation features of GC PDOs in response to chemotherapeutics

Whole-exome sequencing was performed to examine the mutational profiles of organoids in response to chemotherapeutic drugs. There was no significant difference in gene mutations between 5-FU-sensitive and 5-FU-resistant organoids, including the well-known mutations of *ARID1A*, *TP53*, *KRAS*, *CDH1*, and *PIK3CA* in GC (Figure S4A), while more mutations were present

CellPress
OPEN ACCESS

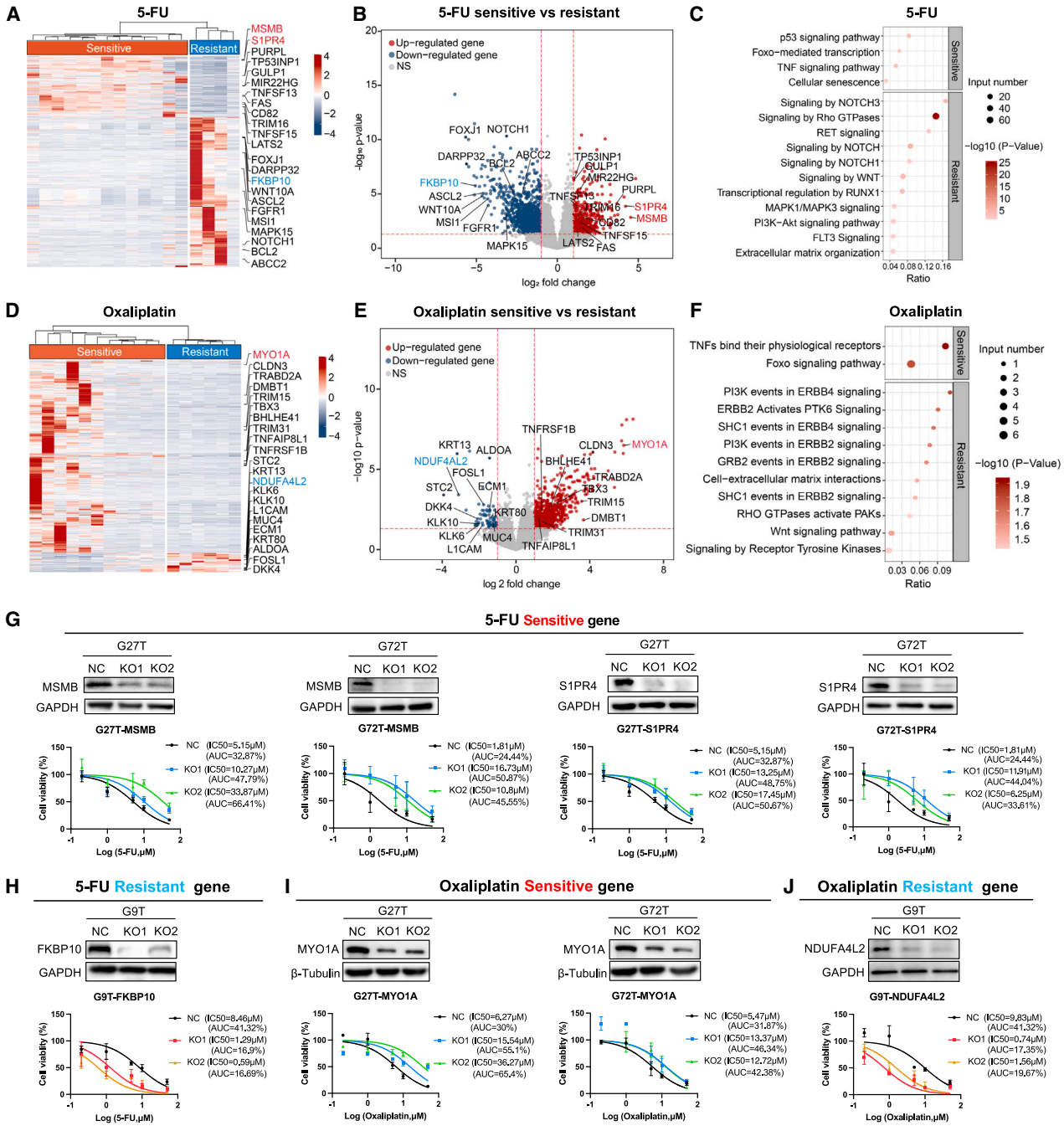

Figure 4. Gene expression signatures of GC PDOs in response to chemotherapeutics

(A) Heatmap and (B) volcano plot analysis showing the most significantly differential genes in 5-FU-sensitive organoids (n = 13) compared to organoids with 5-FU resistance (n = 4). The colored bar represents the log2-transformed values. Individual genes are denoted by gene name. Differentially expressed genes ($p < 0.05$, log2 (fold change) > 1) of 5-FU-sensitive organoids and 5-FU-resistant organoids are indicated in red or blue, respectively.

(C) KOBAS of the differential gene expression profiles of 5-FU-sensitive organoids compared to 5-FU-resistant organoids.

(D and E) Heatmaps and volcano plot analysis showing the most significantly differential enriched genes in oxaliplatin-sensitive organoids (n = 11) compared to organoids with oxaliplatin resistance (n = 6).

(F) KOBAS of the differential gene expression profiles of oxaliplatin-sensitive organoids compared to oxaliplatin-resistant organoids.

(G) Knockout of 5-FU-sensitive gene *MSMB* and *S1PR4* in G27T and G72T organoids (n = 3).

(H) Knockout of 5-FU-resistant gene *FKBP10* in G9T organoids (n = 3).

(I) Knockout of oxaliplatin-sensitive gene *MYO1A* in G27T and G72T organoids (n = 3).

(J) Knockout of oxaliplatin-resistant gene *NDUFA4L2* in G9T organoids (n = 3).

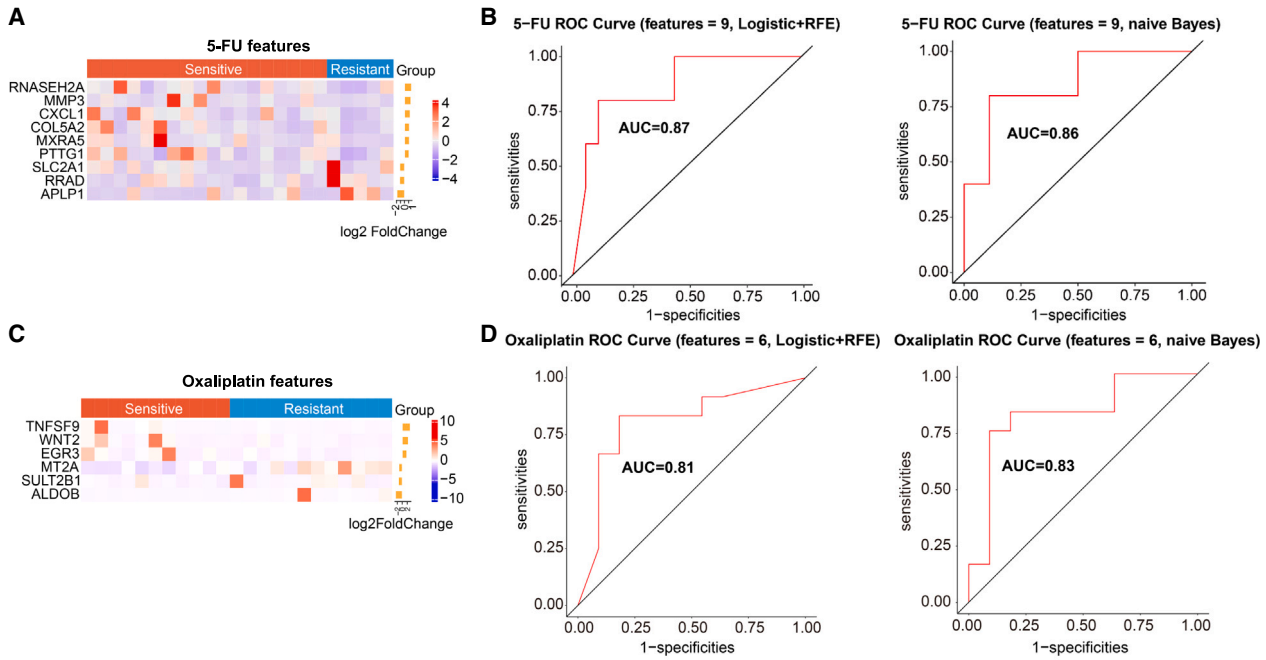

Figure 5. Gene expression biomarkers to distinguish sensitive and resistant responses to chemosensitivity in patients with GC

(A) Heatmap showing a total of 9 genes with significant differential expression between 5-FU-sensitive patients (n = 18) and 5-FU-resistant patients (n = 5). The orange bar represents the log2-transformed fold change values.

(B) Receiver operating characteristic (ROC) analysis to discriminate 5-FU sensitivity and resistance using the 9 differentially expressed genes based on the logistic model (left) or the naive Bayes model (right).

(C) Heatmap showing a total of 6 genes with significant differential expression between oxaliplatin-sensitive patients (n = 11) and oxaliplatin-resistant patients (n = 12).

(D) ROC analysis to discriminate oxaliplatin sensitivity and resistance using the 6 differentially expressed genes based on the logistic model (left) or the naive Bayes model (right). FC, fold change; RFE, recursive feature elimination; ROC, receiver operating characteristic.

in the oxaliplatin-sensitive group than those in the oxaliplatin-resistant group, with *MUC6*, *ARID1A*, and *RIMS2* being the top three most frequently occurred mutations (Figure S4B).

Gene expression biomarkers to distinguish sensitive and resistant responses to chemosensitivity in patients with GC

We then explored gene expression biomarkers of tumor tissues that could distinguish sensitive patients from resistant patients to 5-FU treatment by the recursive feature elimination algorithm. A total of 9 genes with significant differential expression were identified including 6 upregulated genes (*RNASEH2A*, *MMP3*, *CXCL1*, *COL5A2*, *MXRA5*, and *PTTG1*) and 3 downregulated genes (*SLC2A1*, *RRAD*, and *APLP1*) in tumor tissues with 5-FU-sensitive patients compared to those with 5-FU-resistant patients (Figure 5A). We then utilized these 9 genes to verify accuracy by using logistic and naive Bayes models. The results showed that this gene expression biomarker panel could discriminate between 5-FU-sensitive patients and resistant patients at AUCs of 87% (95% confidence interval (CI): 72.22%–100%) by the logistic model and 86% (95% CI: 64.42%–100%) by the naive Bayes model (Figure 5B).

A similar analysis was performed to identify the gene expression biomarkers of tumor tissues to distinguish sensitive patients from resistance patients to oxaliplatin treatment. A total of 6 differentially expressed genes were identified including 3 upregulated genes (*TNFSF9*, *WNT2*, and *EGR3*) and 3 downregulated genes (*MT2A*, *SULT2B1*, and *ALDOB*) in tumor tissues with oxaliplatin-sensitive patients compared to those with oxaliplatin-resistant patients (Figure 5C). This gene expression biomarker panel was further validated by using logistic and naive Bayes models, and the results showed that this panel could discriminate between sensitive patients and resistant patients to oxaliplatin treatment at AUCs of 81% (95% CI: 59.85%–98.48%) by the logistic model and 83% (95% CI: 60.61%–99.24%) by the naive Bayes model (Figure 5D). These findings suggested that the gene expression biomarker panel could distinguish sensitive patients from resistant patients to chemotherapies of 5-FU and oxaliplatin.

Additionally, we verified this gene signature in another cohort (The Cancer Genome Atlas [TCGA]) and analyzed its correlation with survival curves. We screened patients treated with 5-FU or oxaliplatin in TCGA cohort as our validation sets. Patients in the sets were assigned to sensitive-like and resistant-like groups by their gene signature expression level. Survival analysis showed that in the 5-FU-treated cohort (n = 68), patients assigned to the sensitive group had a better prognosis for progression-free survival ($p < 0.05$) (Figure S5A). Due to the limited number of patients receiving oxaliplatin treatment in TCGA set (n = 17), we were unable to identify significant differences in prognosis

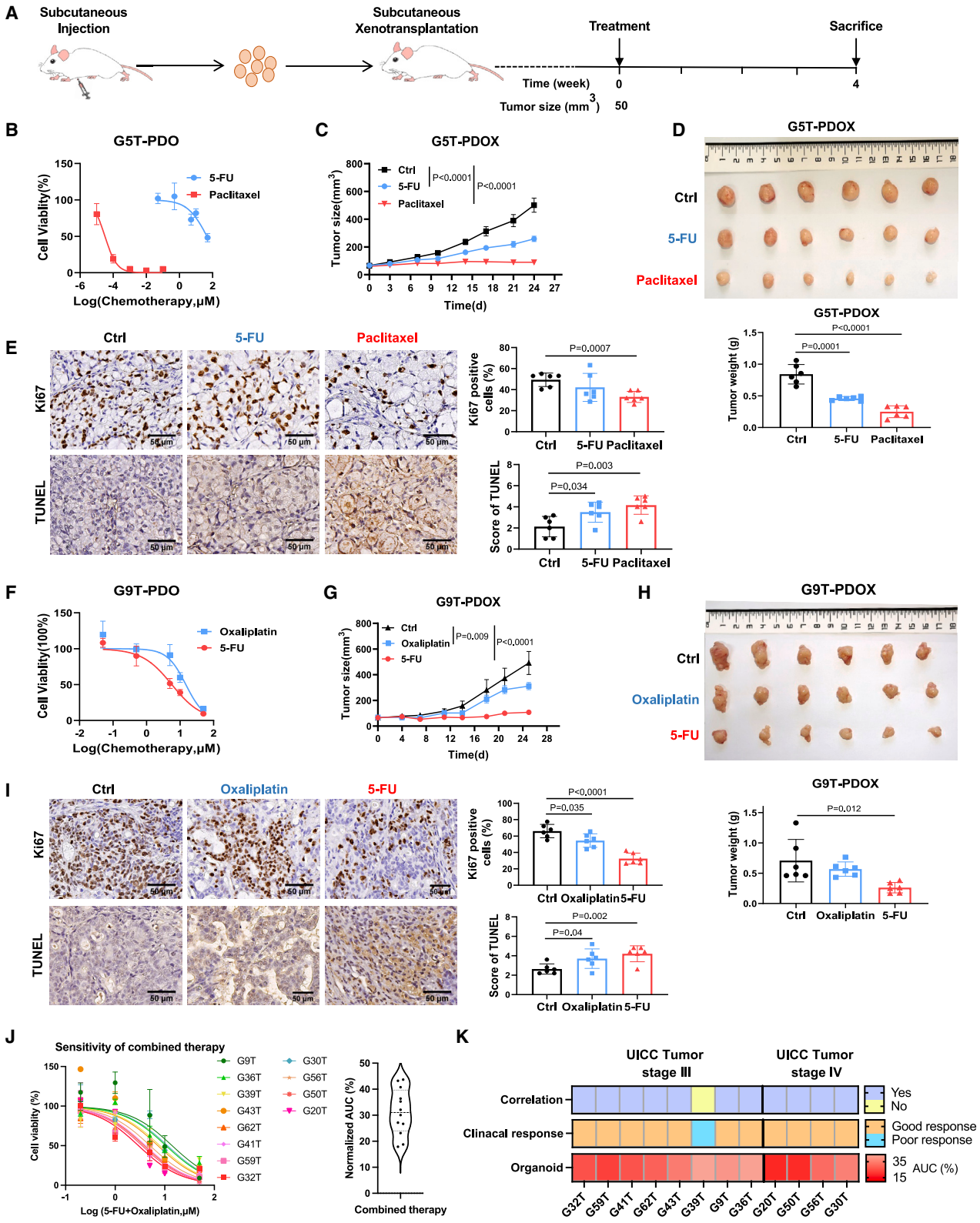

(legend on next page)

between the two groups (Figure S5B). We have compared our gene expression biomarker panel with other panels published, such as 30-gene signature,[16] 53-gene signature,[17] and 32-gene signature,[18] in our dataset by using logistic and naive Bayes models. Our biomarker panels for 5-FU and oxaliplatin have the highest AUC values in both models, thereby confirming the effectiveness of the panels in our study (Figure S6A and S6B).

Drug-response status observed in GC PDOs is validated in PDOXs in mice

To validate the drug-response results identified in GC PDOs, we established PDOXs in NCG mice. Mice were first implanted with different lines of GC organoids. Once the tumors grew larger than 50 mm^3, all mice were randomized to receive either drug or vehicle treatment for 28 days (Figure 6A). G5T-PDOs were sensitive to paclitaxel and resistant to 5-FU (Figure 6B). Consistently, mice engrafted with G5T-PDOXs demonstrated a significant treatment response to paclitaxel ($p < 0.0001$), as evidenced by significantly reduced tumor growth (Figure 6C) and tumor weight (Figure 6D) as compared to untreated G5T-PDOXs. Moreover, G5T-PDOX mice showed resistance to 5-FU treatment, consistent with the result of G5T-PDOs (Figure 6B). In supporting this, cellular proliferation was significantly decreased ($p < 0.001$) and apoptosis was significantly increased ($p < 0.01$) in G5T-PDOXs treated with paclitaxel compared to untreated controls, whereas no difference was observed in the 5-FU treatment group (Figure 6E). In addition, G9T-PDOs were assessed, which were sensitive to 5-FU and resistant to oxaliplatin (Figure 6F). As expected, mice engrafted with G9T-PDOXs demonstrated a significant treatment response to 5-FU ($p < 0.0001$) but no response to oxaliplatin treatment (Figures 6G and 6H). Following 5-FU treatment, cellular proliferation was significantly decreased ($p < 0.0001$) and apoptosis significantly increased ($p < 0.01$) in G9T-PDOXs compared to untreated G9T-PDOXs, whereas no difference was observed in the oxaliplatin treatment group (Figure 6I). G27T-PDOs were sensitive to 5-FU, oxaliplatin, and paclitaxel (Figure S7A). Consistently, mice engrafted with G27T-PDOXs demonstrated a significant treatment response to 5-FU, oxaliplatin, and paclitaxel ($p < 0.0001$), as evidenced by significantly reduced tumor growth and tumor weight (Figures S7B and S7C) as compared to untreated G27T-PDOXs. G30T-PDOs were assessed as sensitive to oxaliplatin and paclitaxel but partially resistant to 5-FU (Figure S7D). As expected, mice engrafted with G30T-PDOXs demonstrated a significantly better response to oxaliplatin and paclitaxel ($p < 0.0001$) than untreated G30T-PDOXs, but a partial response to 5-FU treatment (Figures S7E and S7F). Besides, G72T-PDOXs were sensitive to 5-FU, oxaliplatin, and SN-38, consistent with the drug test result of G72T-PDOs (Figures S7G–S7I). These findings suggested that drug responses observed in GC organoid cultures were validated in PDOXs *in vivo*.

Drug-response status observed in GC PDOs is validated in corresponding follow-up patients with GC

We further validated the drug-sensitive or resistant results from GC PDOs in patients with GC with actual clinical treatment and outcomes. Twelve original patients with GC who underwent chemotherapy and had the combined drug screening results from their derived organoids were followed up (Figures 6J and 6K; Table S4). These patients received perioperative or postoperative adjuvant chemotherapy with oxaliplatin and 5-FU and were followed up for 1–49 months. According to CheckMate 649 trial,[19] which explored chemotherapy of advanced GC, the median progression-free survival time in the observation group is 6.05 months. Thus, a patient who had a recurrence within 6.05 months was defined as a clinically poor responder to chemotherapy. We found that 11 out of 12 (91.7%) patients with GC showed consistent results of drug response as observed in their derived PDOs (Figure 6K; Table S4). For example, patient G32T, who was diagnosed with locally advanced GC and received postoperative adjuvant chemotherapy with oxaliplatin and S-1, had been followed for 35 months with tumor-free survival. In keeping with the actual clinical response, organoids derived from G32T were also sensitive to combined therapy. Thus, drug responses in GC PDOs could be validated in their corresponding follow-up patients with GC, indicating that GC PDOs are useful tools for drug screening and prediction of drug response in patients.

The organoid model as a platform to investigate interaction between cells of the tumor microenvironment and tumor cells

To explore the possibility of co-culturing organoids with fibroblasts cells, we co-cultured GC organoids (G83T and G84T) and matched cancer-associated fibroblasts (CAFs). CAFs grew longer and gradually formed a net-like structure that encircled organoids after 3 days (Figure 7A). On the other hand, co-culture with CAFs significantly enlarged the size of organoids after

Figure 6. Drug-response status observed in GC PDOs is validated in PDOXs in mice and corresponding follow-up patients with GC

(A) Schematic of the mouse experiment.

(B) Dose-response curves of 5-FU (AUC = 68.61%, IC50 = 39.22 μM) and paclitaxel (AUC = 4.32%, IC50 = 0.03 nM) in G5T-PDO *in vitro* ($n = 3$).

(C) Mean tumor size (mm^3) of G5T-PDOX with 5-FU, paclitaxel, or vehicle control over time ($n = 6$ per group) (mean ± SD).

(D) Images of G5T-PDOX tumors and tumor weight at sacrifice.

(E) Representative Ki-67 staining and TUNEL staining of mice tumor sections with quantitative analysis of Ki-67 index (top) and Allred score for apoptosis (bottom) ($n = 6$), respectively. Scale bar, 50 μm.

(F) Dose-response curves of 5-FU (AUC = 31.13%, IC50 = 6.136 μM) and oxaliplatin (AUC = 47.37%, IC50 = 17.53 μM) in G9T-PDO *in vitro* ($n = 3$).

(G) Mean tumor size (mm^3) of G9T-PDOX with 5-FU, oxaliplatin, or vehicle control over time ($n = 6$ per group) (mean ± SD).

(H) Images of G9T-PDOX tumors and tumor weight at sacrifice.

(I) Representative Ki-67 staining and TUNEL staining with quantitative analysis ($n = 6$). Scale bar, 50 μm.

(J) Dose-response curves showing the chemosensitivity of 12 GC organoids to combined chemotherapeutics (5-FU and oxaliplatin). AUC from dose-response data is displayed as a violin plot; every point indicates 12 GC organoids, respectively.

(K) The heatmap summarizes the results for the 12 PDOs and corresponding patient drug responses.

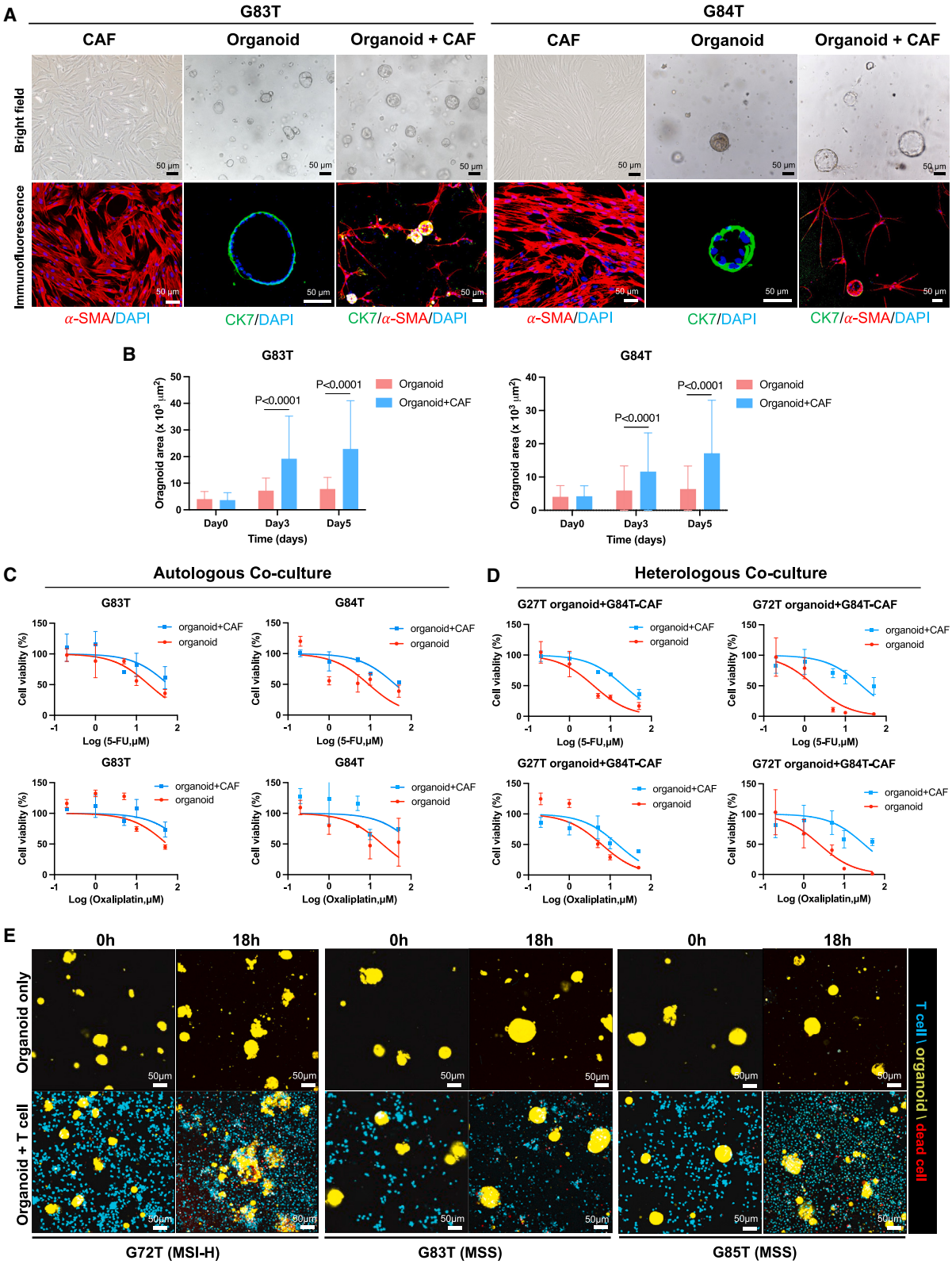

(legend on next page)

5 days (Figures 7B and S8). We then examined the effects of CAFs on tumor organoids in response to 5-FU and oxaliplatin. Of note, autologous CAFs had a significant effect on enhancing the drug resistance to 5-FU and oxaliplatin in both organoids (G83T and G84T) (Figure 7C). Consistently, organoids (G27T and G72T) with heterologous CAF co-culture also increased drug resistance compared with organoids alone. These results suggested the impact of CAFs on the organoids in response to chemotherapy (Figure 7D).

Furthermore, to explore the interaction impacts of organoids and immune cells, we then co-cultured GC organoids derived from three patients with GC (G72T in high microsatellite instability [MSI-H], G83T and G85T in microsatellite stable [MSS] status) with autologous T cells. To activate and stimulate T cells, peripheral blood mononuclear cells (PBMCs) were seeded on an anti-CD28-coated plate together with autologous GC organoids dissociated into single cells in 20:1 ratio. After 2 weeks of co-culture and stimulation, the exposure of PBMCs to autologous tumor organoids led to a significant increase of interferon-gamma (IFN-γ) and TNF-α tumor-reactive T cells in G72T patients (MSI-H), a slight increase of IFN-γ and a significant increase of TNF-α tumor-reactive T cells in G83T patients (MSS), and a slight increase of IFN-γ and a decrease of TNF-α tumor-reactive T cells in G85T patients (MSS), as compared to control PBMCs (Figure S9A). The patient-specific tumor-reactive T cells were therefore applied for co-culture assays to evaluate their tumor-killing effects in organoids. Collectively, these data suggest the feasibility of inducing patient-specific tumor-reactive T cell responses by co-culture of PBMCs and autologous tumor organoids. The addition of autologous T cells led to damaged structure and increased apoptosis of G72T organoids by immunofluorescence staining (Figure 7E). Flow cytometry confirmed the increased apoptosis of tumor cells after co-culture with T cells (Figure S9B). Such effect was not observed in organoids G83T and G85T in MSS statuses co-cultured with T cells (Figures 7E and S9B). These experiments allowed us to observe the interactions between cells in the tumor microenvironment and tumor cells, thereby gaining insights into how these interactions impact the response to treatment.

DISCUSSION

Compared to traditional cancer cell lines and patient-derived tumor xenograft models, PDO models preserve the heterogeneity and complexity of the original tumor, better reflecting an individual patient's pathological and genetic characteristics.[8] In our study, we established an organoid biobank of 57 GC organoid lines from surgically excised samples of patients with GC. Our PDOs could greatly preserve the genetic landscape of tissues where they were derived from, allowing accurate recapitulation of the actual GC condition. High-growth-rate PDOs were derived from patients with more advanced GC (TNM stage $\geq$3); hence, it showed significant upregulation of several well-acknowledged oncogenic pathways particularly NOTCH and MAPK signaling in these organoids.[20] These results collectively indicate the potential to activate proliferation- and stemness-related genes and pathways to accelerate cell proliferation in GC organoids, thereby facilitating and maintaining their long-term cultivation.

We found that most of the genes were reasonably well conserved in organoids, except for immune pathways mainly enriched in tissue and metabolic pathways enriched in organoids, which is consistent with previous reports.[15,21] We then assessed the phenotypic characteristics of GC PDOs and confirmed the consistency between organoids and their corresponding tumors tissues. In particular, our results showed that GC PDOs exhibit similar histological features and protein expression as the subtypes of their corresponding primary tumors. The diffuse type of GC is known to have high expression of CK7,[22] whereas organoids derived from diffuse-type tumors also have upregulated CK7 expression. It is well acknowledged that drug response is greatly influenced by genomic alterations and tumor features. Hence, before utilizing organoids for drug screening, it is of importance to ensure that PDOs could accurately mimic the actual physiological condition by retaining the specific structure and function of their primary tumor tissues.

RNA sequencing was performed to identify gene signatures in GC PDOs associated with chemosensitivity or chemoresistance. In organoids sensitive to chemotherapeutics, multiple well-acknowledged tumor suppressors were upregulated, including *TP53INP1*, *MYO1A*, and *DMBT1*, of which their abilities to inhibit GC and induce cell death were previously reported.[23–28] In organoids resistant to chemotherapeutics, several proliferation- and invasion-related genes were enriched (*DARPP32* in 5-FU-resistant PDOs; *L1CAM* in oxaliplatin-resistant PDOs). *DARPP32* could induce tumorigenesis and resistance of GC cells to gefitinib by promoting interaction between epidermal growth factor receptor and receptor tyrosine protein kinase erbB-3,[29,30] while *L1CAM* is a well-established marker associated with poor prognosis in patients with GC and it could accelerate GC progression and metastasis.[31] Our analysis also identified the upregulation of PI3K and WNT signaling in chemoresistant PDOs. The dysregulation of WNT/β-catenin signaling pathway is critically associated with GC development and chemoresistance.[32,33] Collectively, the gene expression profiles of chemosensitive or chemoresistant organoids were found to be different, and such disparity may at least in part explain the diverse responses among GC PDOs toward chemotherapy.

Figure 7. The organoid model as a platform to investigate interaction between cells of the tumor microenvironment and tumor cells

(A) Representative images of bright-field microscopy and immunofluorescence staining of CAFs, organoids, and co-cultures were immunostained using antibodies against human homologs to show alpha smooth muscle actin (α-SMA) (red) and CK7 (green), respectively. Nuclei are stained with DAPI (blue). Scale bar, 50 μm.

(B) The effect of CAFs on organoid growth on day 0, 3, and 5.

(C and D) Dose-response curves showing chemosensitivity of organoid and organoid with autologous or heterologous CAF co-culture to 2 chemotherapeutics (5-FU and oxaliplatin) (n = 3).

(E) 3D multispectral images of T cells (blue) and GC organoid (yellow) co-cultures at the indicated time points. Scale bar, 50 μm.

Given that gene expression signatures are different between chemosensitive and chemoresistant patients, we therefore evaluated whether these gene biomarkers could be used for the discrimination of chemotherapy response. Our results demonstrated that the top differentially expressed genes accurately discriminate between chemosensitivity and chemoresistance with AUC over 80%, a performance considered as clinically satisfactory.[34] In practice, selecting appropriate therapeutics is crucial for patients; hence, it is of importance to develop a strategy that can accurately and effectively predict treatment outcomes in each patient. A previous study reported that intratumoral infiltration of immune cells including $CD3^+$ and $CD8^+$ cells is a signature for predicting chemotherapy response in patients with GC.[35] Here, we instead revealed the feasibility of utilizing gene signatures to predict chemotherapy outcomes in patients with GC. Notably, further validation of these gene signatures on human samples and patients is necessary prior to clinical application.

Furthermore, PDO models more closely mimic the *in vivo* tumor microenvironment, including cell-cell interactions and extracellular matrix, and can be co-cultured with immune cells, fibroblasts, and other cell types. Hence, it provides a more reliable platform for drug screening.[10] In our study, we demonstrated that GC PDOs are effective tools for drug screening with varied responses to different conventional chemotherapeutics and combination treatment with multiple drugs.

To validate the drug screening results of PDOs, we established a PDOX mouse model using organoids derived from five patients with GC. As expected, consistent responses to chemotherapeutic drugs were observed between PDOX mice and GC PDOs, indicating that *in vitro* organoid cultures could model *in vivo* drug responses. We then testified the drug screening results of PDOs in patients with GC. Over 90% of patients with GC showed consistent results of drug response as observed in their derived PDOs, suggesting the potential of PDOs as tools for predicting drug response in patients with GC. These findings are in line with previous studies using PDOs to predict drug responses in patients with GC, but with smaller sample sizes.[11–13] Moreover, each organoid screening process took less than 2 weeks. This quick turnaround time undoubtedly enables rapid testing in real clinical scenarios. Importantly, we are able to establish organoids using GC biopsies by gastrointestinal endoscopy or puncture. Organoids can assist in identifying potential and appropriate drugs, thereby preventing overtreatment and minimizing treatment-related side effects. Currently, it is an effective tool to be instrumental for those patients.

The interaction between cells of the tumor microenvironment and tumor cells is crucial to understand (and predict) response to treatment. Previous studies have suggested that CAFs secrete a variety of growth factors to regulate cancer development, such as transforming growth factor β, epidermal growth factors, and fibroblast growth factors.[36] Here, we established an organoid-CAF-co-culture system, and found that the CAFs promoted the growth of organoids and drug resistance. The system, which could provide more predictive models, demonstrates that the direct contact between CAFs and cancer cells plays a critical role in tumor progression. Furthermore, we also performed co-culture assays of autologous T cells and organoids and showed that the organoids from patients with MSI-H are more likely to be killed by autologous T cells, demonstrating that tumor organoids can be used to establish personalized model systems to support T cell-based therapies, which is consistent with previous reports.[37]

In conclusion, we established a collection of patient-derived GC organoids that retain the structural and functional characteristics of their originated tumors. These organoids reflected the actual response to chemotherapy in patients, indicating that they could be utilized for the prediction of treatment response in individual patients. Assessing chemosensitivity in organoids can be used as a robust tool for the personalized selection of chemotherapeutic drugs in patients with GC.

Limitations of the study

A prospective study involving a large cohort of GC organoids is necessary before considering implementation in clinical cancer care. The clinical implications and translational potential of our findings necessitate further mechanistic studies and validation in larger patient cohorts.

STAR★METHODS

Detailed methods are provided in the online version of this paper and include the following:

- KEY RESOURCES TABLE
- RESOURCE AVAILABILITY
  - Lead contact
  - Materials availability
  - Data and code availability
- EXPERIMENTAL MODEL AND STUDY PARTICIPANT DETAILS
  - Human gastric cancer tissues
  - PDOX models and chemotherapy in NCG mice
- METHOD DETAILS
  - Establishment of organoid cultures
  - Histology, immunohistochemistry and immunofluorescence
  - Drug screening and cell viability assay
  - Whole-exome sequencing and analysis
  - RNA-sequencing and analysis
  - CRISPR-Cas9 knockout of gene
  - Co-culture of tumor organoids and CAFs
  - T cells and organoid co-culture assays
  - Flow cytometry
- QUANTIFICATION AND STATISTICAL ANALYSIS

SUPPLEMENTAL INFORMATION

Supplemental information can be found online at https://doi.org/10.1016/j.xcrm.2024.101627.

ACKNOWLEDGMENTS

This work was supported by the National Natural Science Foundation of China (82173191), the Guangdong Basic and Applied Basic Research Foundation (2019B151502009), and Kelin Outstanding Young Scientist of the First Affiliated Hospital of Sun Yat-sen University (Y12002).

AUTHOR CONTRIBUTIONS

Y.Z. and L.Z. performed the experiments and drafted the manuscript. S.L. and M.H. performed bioinformatic analysis. Y.X. supervised and commented on bioinformatic analyses. X.S. and Z.C. collected samples and commented on the study. H.C.-H.L. revised the manuscript. J.J.-Y.S. supervised and

commented on the study. L.X., X.L., and J.Y. designed and supervised the study and revised the manuscript.

DECLARATION OF INTERESTS

The authors declare no competing interests.

Received: April 14, 2023
Revised: March 16, 2024
Accepted: June 7, 2024
Published: July 3, 2024

REFERENCES

1. Sung, H., Ferlay, J., Siegel, R.L., Laversanne, M., Soerjomataram, I., Jemal, A., and Bray, F. (2021). Global Cancer Statistics 2020: GLOBOCAN Estimates of Incidence and Mortality Worldwide for 36 Cancers in 185 Countries. CA. Cancer J. Clin. *71*, 209–249. https://doi.org/10.3322/caac.21660.
2. Smyth, E.C., Nilsson, M., Grabsch, H.I., van Grieken, N.C., and Lordick, F. (2020). Gastric cancer. Lancet *396*, 635–648. https://doi.org/10.1016/S0140-6736(20)31288-5.
3. Lordick, F., Carneiro, F., Cascinu, S., Fleitas, T., Haustermans, K., Piessen, G., Vogel, A., and Smyth, E.C.; ESMO Guidelines Committee Electronic address clinicalguidelines@esmoorg (2022). Gastric cancer: ESMO Clinical Practice Guideline for diagnosis, treatment and follow-up. Ann. Oncol. *33*, 1005–1020. https://doi.org/10.1016/j.annonc.2022.07.004.
4. Yoshida, K., Kodera, Y., Kochi, M., Ichikawa, W., Kakeji, Y., Sano, T., Nagao, N., Takahashi, M., Takagane, A., Watanabe, T., et al. (2019). Addition of Docetaxel to Oral Fluoropyrimidine Improves Efficacy in Patients With Stage III Gastric Cancer: Interim Analysis of JACCRO GC-07, a Randomized Controlled Trial. J. Clin. Oncol. *37*, 1296–1304. https://doi.org/10.1200/JCO.18.01138.
5. GASTRIC Global Advanced/Adjuvant Stomach Tumor Research International Collaboration Group; Paoletti, X., Oba, K., Burzykowski, T., Michiels, S., Ohashi, Y., Pignon, J.P., Rougier, P., Sakamoto, J., Sargent, D., et al. (2010). Benefit of adjuvant chemotherapy for resectable gastric cancer: a meta-analysis. JAMA *303*, 1729–1737. https://doi.org/10.1001/jama.2010.534.
6. Kang, Y.K., Chin, K., Chung, H.C., Kadowaki, S., Oh, S.C., Nakayama, N., Lee, K.W., Hara, H., Chung, I.J., Tsuda, M., et al. (2020). S-1 plus leucovorin and oxaliplatin versus S-1 plus cisplatin as first-line therapy in patients with advanced gastric cancer (SOLAR): a randomised, open-label, phase 3 trial. Lancet Oncol. *21*, 1045–1056. https://doi.org/10.1016/S1470-2045(20)30315-6.
7. Al-Batran, S.E., Homann, N., Pauligk, C., Goetze, T.O., Meiler, J., Kasper, S., Kopp, H.G., Mayer, F., Haag, G.M., Luley, K., et al. (2019). Perioperative chemotherapy with fluorouracil plus leucovorin, oxaliplatin, and docetaxel versus fluorouracil or capecitabine plus cisplatin and epirubicin for locally advanced, resectable gastric or gastro-oesophageal junction adenocarcinoma (FLOT4): a randomised, phase 2/3 trial. Lancet *393*, 1948–1957. https://doi.org/10.1016/S0140-6736(18)32557-1.
8. Vlachogiannis, G., Hedayat, S., Vatsiou, A., Jamin, Y., Fernández-Mateos, J., Khan, K., Lampis, A., Eason, K., Huntingford, I., Burke, R., et al. (2018). Patient-derived organoids model treatment response of metastatic gastrointestinal cancers. Science *359*, 920–926. https://doi.org/10.1126/science.aao2774.
9. Yao, Y., Xu, X., Yang, L., Zhu, J., Wan, J., Shen, L., Xia, F., Fu, G., Deng, Y., Pan, M., et al. (2020). Patient-Derived Organoids Predict Chemoradiation Responses of Locally Advanced Rectal Cancer. Cell Stem Cell *26*, 17–26.e6. https://doi.org/10.1016/j.stem.2019.10.010.
10. Shamir, E.R., and Ewald, A.J. (2014). Three-dimensional organotypic culture: experimental models of mammalian biology and disease. Nat. Rev. Mol. Cell Biol. *15*, 647–664. https://doi.org/10.1038/nrm3873.
11. Yan, H.H.N., Siu, H.C., Law, S., Ho, S.L., Yue, S.S.K., Tsui, W.Y., Chan, D., Chan, A.S., Ma, S., Lam, K.O., et al. (2018). A Comprehensive Human Gastric Cancer Organoid Biobank Captures Tumor Subtype Heterogeneity and Enables Therapeutic Screening. Cell Stem Cell *23*, 882–897.e11. https://doi.org/10.1016/j.stem.2018.09.016.
12. Seidlitz, T., Merker, S.R., Rothe, A., Zakrzewski, F., von Neubeck, C., Grützmann, K., Sommer, U., Schweitzer, C., Schölch, S., Uhlemann, H., et al. (2019). Human gastric cancer modelling using organoids. Gut *68*, 207–217. https://doi.org/10.1136/gutjnl-2017-314549.
13. Steele, N.G., Chakrabarti, J., Wang, J., Biesiada, J., Holokai, L., Chang, J., Nowacki, L.M., Hawkins, J., Mahe, M., Sundaram, N., et al. (2019). An Organoid-Based Preclinical Model of Human Gastric Cancer. Cell. Mol. Gastroenterol. Hepatol. *7*, 161–184. https://doi.org/10.1016/j.jcmgh.2018.09.008.
14. Tiriac, H., Belleau, P., Engle, D.D., Plenker, D., Deschènes, A., Somerville, T.D.D., Froeling, F.E.M., Burkhart, R.A., Denroche, R.E., Jang, G.H., et al. (2018). Organoid Profiling Identifies Common Responders to Chemotherapy in Pancreatic Cancer. Cancer Discov. *8*, 1112–1129. https://doi.org/10.1158/2159-8290.CD-18-0349.
15. Schütte, M., Risch, T., Abdavi-Azar, N., Boehnke, K., Schumacher, D., Keil, M., Yildiriman, R., Jandrasits, C., Borodina, T., Amstislavskiy, V., et al. (2017). Molecular dissection of colorectal cancer in pre-clinical models identifies biomarkers predicting sensitivity to EGFR inhibitors. Nat. Commun. *8*, 14262. https://doi.org/10.1038/ncomms14262.
16. Na, D., Chae, J., Cho, S.Y., Kang, W., Lee, A., Min, S., Kang, J., Kim, M.J., Choi, J., Lee, W., et al. (2021). Predictive biomarkers for 5-fluorouracil and oxaliplatin-based chemotherapy in gastric cancers via profiling of patient-derived xenografts. Nat. Commun. *12*, 4840. https://doi.org/10.1038/s41467-021-25122-4.
17. Zhu, L., Wang, H., Jiang, C., Li, W., Zhai, S., Cai, X., Wang, X., Liao, L., Tao, F., Jin, D., et al. (2020). Clinically applicable 53-Gene prognostic assay predicts chemotherapy benefit in gastric cancer: A multicenter study. EBioMedicine *61*, 103023. https://doi.org/10.1016/j.ebiom.2020.103023.
18. Cheong, J.H., Wang, S.C., Park, S., Porembka, M.R., Christie, A.L., Kim, H., Kim, H.S., Zhu, H., Hyung, W.J., Noh, S.H., et al. (2022). Development and validation of a prognostic and predictive 32-gene signature for gastric cancer. Nat. Commun. *13*, 774. https://doi.org/10.1038/s41467-022-28437-y.
19. Janjigian, Y.Y., Shitara, K., Moehler, M., Garrido, M., Salman, P., Shen, L., Wyrwicz, L., Yamaguchi, K., Skoczylas, T., Campos Bragagnoli, A., et al. (2021). First-line nivolumab plus chemotherapy versus chemotherapy alone for advanced gastric, gastro-oesophageal junction, and oesophageal adenocarcinoma (CheckMate 649): a randomised, open-label, phase 3 trial. Lancet *398*, 27–40. https://doi.org/10.1016/S0140-6736(21)00797-2.
20. Hibdon, E.S., Razumilava, N., Keeley, T.M., Wong, G., Solanki, S., Shah, Y.M., and Samuelson, L.C. (2019). Notch and mTOR Signaling Pathways Promote Human Gastric Cancer Cell Proliferation. Neoplasia *21*, 702–712. https://doi.org/10.1016/j.neo.2019.05.002.
21. Farin, H.F., Mosa, M.H., Ndreshkjana, B., Grebbin, B.M., Ritter, B., Menche, C., Kennel, K.B., Ziegler, P.K., Szabó, L., Bollrath, J., et al. (2023). Colorectal Cancer Organoid-Stroma Biobank Allows Subtype-Specific Assessment of Individualized Therapy Responses. Cancer Discov. *13*, 2192–2211. https://doi.org/10.1158/2159-8290.CD-23-0050.
22. Dixon, K., Brew, T., Farnell, D., Godwin, T.D., Cheung, S., Chow, C., Ta, M., Ho, G., Bui, M., Douglas, J.M., et al. (2021). Modelling hereditary diffuse gastric cancer initiation using transgenic mouse-derived gastric organoids and single-cell sequencing. J. Pathol. *254*, 254–264. https://doi.org/10.1002/path.5675.
23. Seillier, M., Peuget, S., Gayet, O., Gauthier, C., N'Guessan, P., Monte, M., Carrier, A., Iovanna, J.L., and Dusetti, N.J. (2012). TP53INP1, a tumor suppressor, interacts with LC3 and ATG8-family proteins through the LC3-interacting region (LIR) and promotes autophagy-dependent cell death. Cell Death Differ. *19*, 1525–1535. https://doi.org/10.1038/cdd.2012.30.

24. Wang, M., Gu, H., Qian, H., Zhu, W., Zhao, C., Zhang, X., Tao, Y., Zhang, L., and Xu, W. (2013). miR-17-5p/20a are important markers for gastric cancer and murine double minute 2 participates in their functional regulation. Eur. J. Cancer *49*, 2010–2021. https://doi.org/10.1016/j.ejca.2012.12.017.

25. Mazzolini, R., Dopeso, H., Mateo-Lozano, S., Chang, W., Rodrigues, P., Bazzocco, S., Alazzouzi, H., Landolfi, S., Hernández-Losa, J., Andretta, E., et al. (2012). Brush border myosin Ia has tumor suppressor activity in the intestine. Proc. Natl. Acad. Sci. USA *109*, 1530–1535. https://doi.org/10.1073/pnas.1108411109.

26. Mazzolini, R., Rodrigues, P., Bazzocco, S., Dopeso, H., Ferreira, A.M., Mateo-Lozano, S., Andretta, E., Woerner, S.M., Alazzouzi, H., Landolfi, S., et al. (2013). Brush border myosin Ia inactivation in gastric but not endometrial tumors. Int. J. Cancer *132*, 1790–1799. https://doi.org/10.1002/ijc.27856.

27. Mollenhauer, J., Herbertz, S., Helmke, B., Kollender, G., Krebs, I., Madsen, J., Holmskov, U., Sorger, K., Schmitt, L., Wiemann, S., et al. (2001). Deleted in Malignant Brain Tumors 1 is a versatile mucin-like molecule likely to play a differential role in digestive tract cancer. Cancer Res. *61*, 8880–8886.

28. Koopaie, M., Ghafourian, M., Manifar, S., Younespour, S., Davoudi, M., Kolahdooz, S., and Shirkhoda, M. (2022). Evaluation of CSTB and DMBT1 expression in saliva of gastric cancer patients and controls. Cancer *22*, 473. https://doi.org/10.1186/s12885-022-09570-9.

29. Chen, Z., Zhu, S., Hong, J., Soutto, M., Peng, D., Belkhiri, A., Xu, Z., and El-Rifai, W. (2016). Gastric tumour-derived ANGPT2 regulation by DARPP-32 promotes angiogenesis. Gut *65*, 925–934. https://doi.org/10.1136/gutjnl-2014-308416.

30. Zhu, S., Belkhiri, A., and El-Rifai, W. (2011). DARPP-32 increases interactions between epidermal growth factor receptor and ERBB3 to promote tumor resistance to gefitinib. Gastroenterology *141*, 1738–1748.e482. https://doi.org/10.1053/j.gastro.2011.06.070.

31. Chen, D.L., Zeng, Z.L., Yang, J., Ren, C., Wang, D.S., Wu, W.J., and Xu, R.H. (2013). L1cam promotes tumor progression and metastasis and is an independent unfavorable prognostic factor in gastric cancer. J. Hematol. Oncol. *6*, 43. https://doi.org/10.1186/1756-8722-6-43.

32. Yu, S., Li, L., Cai, H., He, B., Gao, Y., and Li, Y. (2021). Overexpression of NELFE contributes to gastric cancer progression via Wnt/β-catenin signaling-mediated activation of CSNK2B expression. J. Exp. Clin. Cancer Res. *40*, 54. https://doi.org/10.1186/s13046-021-01848-3.

33. Min, J., Zhang, C., Bliton, R.J., Caldwell, B., Caplan, L., Presentation, K.S., Park, D.J., Kong, S.H., Lee, H.S., Washington, M.K., et al. (2022). Dysplastic Stem Cell Plasticity Functions as a Driving Force for Neoplastic Transformation of Precancerous Gastric Mucosa. Gastroenterology *163*, 875–890. https://doi.org/10.1053/j.gastro.2022.06.021.

34. Mandrekar, J.N. (2010). Receiver operating characteristic curve in diagnostic test assessment. J. Thorac. Oncol. *5*, 1315–1316. https://doi.org/10.1097/JTO.0b013e3181ec173d.

35. Jiang, Y., Xie, J., Huang, W., Chen, H., Xi, S., Han, Z., Huang, L., Lin, T., Zhao, L.Y., Hu, Y.F., et al. (2019). Tumor Immune Microenvironment and Chemosensitivity Signature for Predicting Response to Chemotherapy in Gastric Cancer. Cancer Immunol. Res. *7*, 2065–2073. https://doi.org/10.1158/2326-6066.CIR-19-0311.

36. Liu, J., Li, P., Wang, L., Li, M., Ge, Z., Noordam, L., Lieshout, R., Verstegen, M.M.A., Ma, B., Su, J., et al. (2021). Cancer-Associated Fibroblasts Provide a Stromal Niche for Liver Cancer Organoids That Confers Trophic Effects and Therapy Resistance. Cell. Mol. Gastroenterol. Hepatol. *11*, 407–431. https://doi.org/10.1016/j.jcmgh.2020.09.003.

37. Dijkstra, K.K., Cattaneo, C.M., Weeber, F., Chalabi, M., van de Haar, J., Fanchi, L.F., Slagter, M., van der Velden, D.L., Kaing, S., Kelderman, S., et al. (2018). Generation of Tumor-Reactive T Cells by Co-culture of Peripheral Blood Lymphocytes and Tumor Organoids. Cell *174*, 1586–1598.e12. https://doi.org/10.1016/j.cell.2018.07.009.

38. Ganesh, K., Wu, C., O'Rourke, K.P., Szeglin, B.C., Zheng, Y., Sauvé, C.E.G., Adileh, M., Wasserman, I., Marco, M.R., Kim, A.S., et al. (2019). A rectal cancer organoid platform to study individual responses to chemoradiation. Nat. Med. *25*, 1607–1614. https://doi.org/10.1038/s41591-019-0584-2.

39. van de Wetering, M., Francies, H.E., Francis, J.M., Bounova, G., Iorio, F., Pronk, A., van Houdt, W., van Gorp, J., Taylor-Weiner, A., Kester, L., et al. (2015). Prospective derivation of a living organoid biobank of colorectal cancer patients. Cell *161*, 933–945. https://doi.org/10.1016/j.cell.2015.03.053.

40. Malta, T.M., Sokolov, A., Gentles, A.J., Burzykowski, T., Poisson, L., Weinstein, J.N., Kamińska, B., Huelsken, J., Omberg, L., Gevaert, O., et al. (2018). Machine Learning Identifies Stemness Features Associated with Oncogenic Dedifferentiation. Cell *173*, 338–354.e15. https://doi.org/10.1016/j.cell.2018.03.034.

STAR★METHODS

KEY RESOURCES TABLE

REAGENT or RESOURCE	SOURCE	IDENTIFIER
Antibodies		
Anti-Cytokeratin 7	Abcam	Cat#ab9021, RRID: AB_306947
Anti-Carcino Embryonic Antigen CEA antibody	Abcam	Cat#ab207718, RRID: AB_3086740
Anti-Prostate Secretory Protein/PSP antibody	Abcam	Cat#ab128897, RRID: AB_11150619
S1P4/EDG-6 Antibody	Novus Biologicals	Cat# NBP2-24500, RRID: AB_3086741
FKBP10/FKBP65 Polyclonal antibody	Proteintech	Cat#12172-1-AP, RRID: AB_2102550
Anti-MYO1A Rabbit Polyclonal Antibody	Proteintech	Cat#17499-1-AP, RRID: AB_2148172
NDUFA4L2 Polyclonal antibody	Proteintech	Cat#16480-1-AP, RRID: AB_2150637
Anti-Ki67	Cell Signaling Technology	Cat#12202S, RRID: AB_2620142
Anti-alpha smooth muscle Actin antibody	Abcam	Cat#ab124964, RRID: AB_11129103
Anti-CD28 Mouse Monoclonal Antibody	BioLegend	Cat#302934, RRID: AB_11148949
BUV395 Mouse Anti-Human CD3	BD Biosciences	Cat#563546, RRID: AB_2744387
BV510 Mouse Anti-Human CD45	BD Biosciences	Cat#563204, RRID: AB_2738067
APC Mouse Anti-Human CD8	BD Biosciences	Cat#566852, RRID: AB_2869906
PE-CY7 Mouse Anti-Human TNF-a	BD Biosciences	Cat#557647, RRID: AB_396764
BV605 Mouse Anti-Human IFN-γ	BD Biosciences	Cat#562974, RRID: AB_2737926
Biological samples		
Human gastric cancer sample	First Affiliated Hospital of Sun Yat-sen University	N/A
Chemicals, peptides, and recombinant proteins		
Cisplatin	Selleck	Cat#S1166
Oxaliplatin	Selleck	Cat#S1224
5-Fluorouracil	Selleck	Cat#S1209
SN-38	Selleck	Cat#S4908
Paclitaxel	Selleck	Cat#S1150
Doxorubicin	Selleck	Cat#S1208
B-27™ Supplement, serum free	Thermo Fisher Scientific	Cat#17504044
GlutaMAX	Gibco	Cat#35050061
HEPES	Gibco	Cat#15630080
Pen/Strep	Gibco	Cat#15140122
N-acetyl-L-cysteine	Sigma	Cat#A9165-5G
Gastrin-1, human	Genscript	Cat#PR12740
Recombinant Human EGF	Peprotech	Cat#AF-100-15
Recombinant Human FGF-10	Peprotech	Cat#100-26
A83-01	TOCRIS	Cat#2939
Y-27632	Selleck	Cat#S1049
Recombinant Human Noggin	Peprotech	Cat#120-10C
Primocin	Invivogen	Cat#ant-pm-1
NucRed Dead 647	Thermo Fisher Scientific	Cat#R37113
Oregon Green™ 488 BAPTA-1	Thermo Fisher Scientific	Cat#O6807
eBioscience Cell Proliferation Dye eFluor 450	Thermo Fisher Scientific	Cat#65-0842-90
CellEvent™ Caspase-3/7 Green	Thermo Fisher Scientific	Cat#C10423
Matrigel	Corning	Cat#356231
Advanced DMEM/F-12	Gibco	Cat#12634010

(*Continued on next page*)

Continued

REAGENT or RESOURCE	SOURCE	IDENTIFIER
RPMI 1640	Gibco	Cat#11875168
Collagenase type IV	Gibco	Cat#17104019
dispase type II	Gibco	Cat#17105041
TrypLE Express	Gibco	Cat#12605010
Fibroblast culture medium	iCELL	Cat#PriMed-iCELL-003
Stain Buffer	BD Pharmingen™	Cat#554656
Critical commercial assays		
TUNEL apoptosis detection kit	KeyGen BioTECH	Cat#KGA700
CellTiter-Glo assay	Promega	Cat#G7570
QIAamp® DNA Mini Kit	Qiagen	Cat#51304
RNeasy Mini Kit	QIAEN	Cat#74104
Deposited data		
Raw and analyzed data	This paper	GSA: HRA006195
Experimental models: Organisms/strains		
NCG (NOD-Prkdc^{em26Cd52}Il2rg^{em26Cd22}/Nju) mice	GemPharmatech, Nanjing, China	Cat#T001475
Oligonucleotides		
MSMB sgRNA-1: AACACCCAATAAACTCGGAG sgRNA-2: ATTGCATAAAGTCACGAAGG	This paper	N/A
S1PR4 sgRNA-1: CGGCCATCACCAGCCACATG sgRNA-2: TGTAGTGCAGAACAATGAGC	This paper	N/A
FKBP10 sgRNA-1: GGCACTTATGACACCTACGT sgRNA-2: TGGAAGATGTGGTCATCGAG	This paper	N/A
MYO1A sgRNA-1: ACATTTACTCACAAATCGGG sgRNA-2: TGTGGCGTACCAGTCACTGA	This paper	N/A
NDUFA4L2 sgRNA-1: GCAGATCAAAAGACATCCGG sgRNA-2: TATGGCAGGAGCCAGTCTTG	This paper	N/A
Software and algorithms		
GraphPad 10.0	GraphPad Software	N/A
ImageJ	NIH	https://imagej.nih.gov/ij/

RESOURCE AVAILABILITY

Lead contact

Further information and requests for resources and reagents should be directed to and will be fulfilled by the lead contact, Prof. Li (lixiaox23@mail.sysu.edu.cn).

Materials availability

This study did not generate new unique reagents.

Data and code availability

The sequencing data reported in this paper are deposited in Genome Sequence Archive (GSA) with project number HRA006195 (https://ngdc.cncb.ac.cn/gsa-human/browse/HRA006195) and will be publicly available as of the date of publication. There are no restrictions on data access for academic use. Requests to access data should follow the GSA's "Data Access Request Guidance" available at https://ngdc.cncb.ac.cn/gsa-human/document. The software and algorithms for data analyses used in this study are published and referenced throughout the STAR Methods section. No original code is featured in this paper. Any additional information required to reanalyze the data reported in this paper is available from the lead contact upon request.

EXPERIMENTAL MODEL AND STUDY PARTICIPANT DETAILS

Human gastric cancer tissues

Fresh tumor tissues were obtained from 73 patients with GC receiving surgical resection (Table S1) at the First Affiliated Hospital of Sun Yat-sen University, Guangzhou, China, from 2019 to 2023. This study was approved by the Clinical Research Ethics Committee of the First Affiliated Hospital of Sun Yat-sen University and conducted in accordance with the Declaration of Helsinki (No. [2020]052). Written informed consent was obtained from all patients.

PDOX models and chemotherapy in NCG mice

Male NCG (NOD-Prkdc^{em26Cd52}Il2rg^{em26Cd22}/Nju) mice were purchased from Gempharmatech Co., Ltd. (Jiangsu, China). For PDOX, digested GC organoids (G5T-PDO, G9T-PDO, G27T-PDO, G30T-PDO, G72T-PDO) were injected subcutaneously into the right dorsal flank of 5-week-old male NCG mice (1×10^6 cells in 100 μL Matrigel/PBS per mouse). Tumor size was measured using a digital caliper every third day, and tumor volume (mm^3) was calculated using the formula: volume = length × width^2 × 0.5. When the tumor size reached 50 mm^3, mice were randomly divided into sensitive, resistant or control groups. Drugs were administered by intraperitoneal injection, including 5-FU (25 mg/kg in 0.9% NaCl, twice a week), oxaliplatin (6 mg/kg in 5% glucose solution, once a week), paclitaxel (10 mg/kg in 0.9% NaCl, once a week), and SN-38 (15 mg/kg in 0.9% NaCl, twice a week). Mice were sacrificed after treatment, and fresh tumors were harvested for subsequent analysis. All experiments were conducted in accordance with the guidelines approved by the Animal Ethics Committee of the First Affiliated Hospital of Sun Yat-sen University.

METHOD DETAILS

Establishment of organoid cultures

Freshly collected tissues were immediately placed in tissue storage solution (MACS). Digested tumor tissues were filtered through a 70 μm filter and centrifugated at 300×g. The cell pellet was resuspended in Matrigel after washing, and a volume of 30 μL Matrigel-cell mixture was seeded per well on a prewarmed 48-well plate. After Matrigel was solidified, 250 μL of complete GC organoid medium was added which consisted of advanced DMEM/F12 (Gibco, 12634010), 1x GlutaMax, 1x HEPES, 40% Wnt3a, 10% RSPO-1, 100 ng/mL Noggin (PeproTech, 120-10C), 1x B27 (Thermo Fisher Scientific, 17504044), 50 ng/mL EGF (PeproTech, AF-100-15), and 100 ng/mL FGF10 (PeproTech, 100-26), 1mM N-Acetylcystenine, 1nM Gastrin, 1μM A83-01, 10 μM Y-27632 and 1μg/ul primocin. The culture medium was replenished every 3–4 days, and organoids were passaged every 1–2 weeks using TrypLE Express (Gibco).

Histology, immunohistochemistry and immunofluorescence

Tissues and organoids were fixed in 4% paraformaldehyde and they were sectioned at a thickness of 4 μm after processing. Hematoxylin and eosin staining was conducted using the standard histological protocol. Immunohistochemistry staining was performed using anti-CK7 antibody (1:1000, Abcam, ab9021), anti-CEA antibody (1:20000, Abcam, ab207718), and anti-Ki67 antibody (1:400, Cell Signaling Technology, 12202S). According to the manufacturer's instructions, TUNEL (terminal deoxynucleotidyl transferase nick-end labeling) staining was performed using an apoptosis detection kit (KeyGen BioTECH, KGA700). Immunofluorescence staining was performed using anti-CK7 antibody, and α-SMA (1:1000, ab124964, Abcam). To quantify staining, five random areas per specimen were captured under microscope with 40× magnification, and the percentage of positively stained cells was determined using ImageJ software.

Drug screening and cell viability assay

GC organoids were harvested and digested into single cells and counted with 0.4% Trypan Blue solution. Organoids were resuspended in advanced DMEM/F12 and Matrigel at a ratio of 1:2 and embedded in 96-well plates (250 cells per 5 μL suspension per well). After Matrigel was solidified, 100 μL of complete medium was added with incubation for 24 h. The complete medium was then replaced with culture medium with different concentrations of chemotherapy drugs, including 5-FU, oxaliplatin, cisplatin, paclitaxel, doxorubicin, and irinotecan active metabolite SN-38 (Selleck, Washington). 10 μM phenylarsine oxide was used as positive control, and dimethyl sulfoxide was used as negative control. Each drug concentration was performed in triplicate. For combined drug treatments, organoids were treated as follows: 5-FU: oxaliplatin, 25:1. Cell viability was assessed using CellTiter-Glo Luminescent Cell Viability Assay (Promega). After 6 days of drug incubation, the luminescence of each well was measured. There were some reports that drug sensitivity was classified by both IC50 and area under the curve (AUC), but these studies focused on relative sensitivity and relative resistance, without a specific cut-off value.[38,39] In this study, we mainly used the AUC value to classify the organoids as resistant (AUC >50%) or sensitive (AUC <50%).

Whole-exome sequencing and analysis

DNA was extracted from paired tumor and adjacent non-tumorous gastric epithelium mucosa as well as PDOs using QIAamp DNA Mini Kit (Qiagen, Germantown, MD). Whole-exome sequencing was performed using HiSeq X TEN platform (Illumina), and the sequencing mean depths were 300x.

Sequencing reads were mapped against human genome build 37 (hg19) by Burrows-Wheeler Aligner (version 0.7.10). The BAM files were further processed in terms of duplicate marking using samtools (version 0.1.19). Local realignment and base recalibration were performed by Genome Analysis Toolkits (GATK v3.2-2). Single-nucleotide polymorphisms and small insertions/deletions were identified by providing the peri-tumor tissues as a reference and their corresponding tumor or organoid sequencing data to MuTect2 (involved in GATK v3.2-2) with default parameters. Filters for Next Generation Sequencing (FiNGS) software was used to generate VCF files with high quality by applying the filtering criteria of International Cancer Genome Consortium (ICGC) to the remaining variants. Annovar was then used to annotate somatic variants with the following databases: gnomAD, dbSNP, ICGC, Catalog of Somatic Mutations in Cancer (COSMIC), ClinVar, dbNSFP and dbscSNV. Mutational signatures were visualized using maftools v2.4.12 (https://bioconductor.org/packages/release/bioc/vignettes/maftools/inst/doc/maftools.html).

RNA-sequencing and analysis

Total RNA was extracted from tumor organoids and tissue using RNeasy Mini Kit (QIAEN, 74104) following the manufacturer's instructions. The amount of extracted RNA was quantified using Agilent 5400 Bioanalyzer. RNA-sequencing was performed using HiSeq X TEN platform (Illumina), and 150-bp paired-end reads were generated. RNA-sequencing data were processed to filter out low quality reads and trim all reads in front and tail using Fastp. The remaining reads were aligned to the human reference genome Hg19 using HISAT2. Gene expression levels were quantified by RNASeQC2 to generate fragments per kilobase of exon model per million mapped fragments (FPKM) and read counts, which were used for pathway enrichment analysis and differential gene expression analysis, respectively. Stemness score was generated according to the reported method.[40] We use the mRNA-based stemness index (mRNAsi) to evaluate the dedifferentiation potential of tumor cells. The stemness score is defined as the Spearman correlation coefficient between the gene expression profile of our samples and the reported expression profile of stem cell features in the article mentioned above. The score ranges between 0 and 1, with a higher value indicating a closer similarity to stem cell expression features, implying a higher degree of stemness. We observed a significant difference between the fast-growing group and the slow-growing group ($p = 0.023$), with an average score of 0.784 for the fast-growing group and 0.345 for the slow-growing group. We use Spearman correlation coefficient (ρ) and R square (R^2) to access the gene expression level (in log2 FPKM) between organoids and their corresponding primary tumor tissues. Spearman correlation coefficient (ρ) was calculated by "cor" function with parameter "method = spearman" in R package stats (v4.2.0) and R square (R^2) was computed by "lm" function in R package stats (v4.2.0). According to the results of *in vitro* drug screening, organoids were separated into either sensitive group (AUC <50%) or resistant group (AUC $\geq$50%). Significantly differentially expressed genes between the two groups were filtered by DESeq2 package in R with read counts ($p < 0.05$, log2-fold change ≥ 1 or ≤ -1) and visualized as volcano plots by R ggplot2. KEGG Orthology Based Annotation System (KOBAS) (http://kobas.cbi.pku.edu.cn/anno_iden.php) was applied to FPKM expression data. Analysis of enriched pathways was annotated using KEGG and Reactome. Recursive feature elimination (RFE) algorithm was then performed for feature ranking and selection. Logistic regression model was performed with LogisticRegression module in Scikit-learn20 (v 0.24.2) python package. Naive Bayes model was performed using e1071 (v 1.7–9, https://cran.r-project.org/package=e1071) R package.

CRISPR-Cas9 knockout of gene

CRISPR-Cas9-mediated knockout was performed with lentiCRISPRv2 system. Briefly, guide RNAs targeting the human genomic locus of *MSMB*, *S1PR4*, *FKBP10*, *MYO1A*, *NDUFA4L2* (sg #1 and #2) were obtained from GenScript and cloned into the lentiCRISPRv2 vector. Lentivirus were then generated by co-transfection of lentiCRISPRv2 vector and packaging plasmids in 293T cells. To perform knockout, GC organoids were harvested and digested into single cells and counted with 0.4% Trypan Blue solution, $2x10^5$ cells were resuspended in medium containing Rho kinase inhibitor Y27632 (10 μM) and Polybrene (8 μg/mL) and CRISPR-Cas9-gRNA lentivirus spinfected (500g, 1 h, 32°C). After 3–5 h of incubation at 37°C, cells were seeded in Matrigel. Puromycin selection was started 3 days after transduction. Puromycin-resistant organoids were isolated and confirmed by western blot.

Co-culture of tumor organoids and CAFs

Human CAFs were isolated from gastric cancer tissues. Tumor tissue was digested with a digestion solution: collagenase type IV (0.25 mg/mL, Gibco), dispase (0.125 mg/mL, Gibco) in Advanced DMEM/F12 (Gibco) for 60 min. Digested tumor tissues were filtered through a 70 μm filter and centrifugated at 300 × g. The pellet was plated in a T25 flask and fibroblast was allowed to grow in fibroblast culture medium (PriMed-iCELL-003, iCELL). The fibroblasts were checked by using immunofluorescence staining of α-SMA (1:1000, ab124964, Abcam).

GC organoids were harvested and digested into single cells and counted with 0.4% Trypan Blue solution. CAFs used for experimental studies at passages 4–6. For co-cultures, CAFs and organoids at a ratio of 1:2 embedded in Matrigel. After Matrigel was solidified, complete medium was added. After co-culturing organoids with CAFs for 5 days, the organoids image was captured and diameters of was measured using ImageJ software on day 0, day 3, day 5, respectively. For drug response, organoids with or without CAFs was treated with 5-FU and oxaliplatin as described above.

T cells and organoid co-culture assays

Fresh peripheral blood was collected with informed consent. The peripheral blood mononuclear cells (PBMC) fraction was isolated from peripheral blood by Ficoll-Paque PLUS density gradient separation, counted and cryopreserved for T cell activation assays. To

expand and activate T cells, PBMCs were seeded on an anti-CD28-coated plate together with autologous GC organoids dissociated into single cells in 20:1 ratio. T cell culture Medium was refreshed every 2 days, which was composed of RPMI 1640 medium supplemented with 1% penicillin/streptomycin, 1% Ultraglutamine I, 1% HEPES, 50 nM β-Mercaptoethanol, 10% fetal bovine serum and 200 U/mL IL-2. After 2 weeks of expansion, T cells were ready for coculture assays to evaluate tumor killing effect.

Organoids for T cell coculture were released from Matrigel by cold PBS and resuspended in GC culture medium. The suspensions were filtered with a 100μm strainer to remove organoids in large size. Activated T cells were cocultured with GC organoids at a ratio of 5:1 for 18 h. Cells were plated in a 96-well, glass-bottom, high content screening microplates (Corning) in 200 μL medium containing 100 μL T cell culture medium and 100 μL GC organoid culture medium. NucRed Dead 647 (two drops per milliliter, Thermo Fisher Scientific) was added for labeling of dead cells. To facilitate visualization, GC organoids were pre-stained with Oregon Green 488 BAPTA-1 (Thermo Fisher Scientific) and T cells with eBioscience Cell Proliferation Dye eFluor 450 (Thermo Fisher Scientific) in RPMI 1640 for 20 min at 37°C, then washed with completed medium for twice. Living cell imaging were performed at 0h and 18h after cell seeding using laser scanning confocal microscope (Olympus FV3000).

Flow cytometry

GC organoids cultured with or without T cells were incubated with CellEvent Caspase-3/7 Green (Thermo Fisher Scientific) to label apoptotic cells and evaluate killing effect by T cells. Organoids were dissociated into single cells using TrypLE Express and washed in stain Buffer (BD Pharmingen, 554656). The cells were then filtered with 70 μm cell strainers and stained with BUV395 Mouse Anti-Human CD3 (BD Biosciences), BV510 Mouse Anti-Human CD45 (BD Biosciences), APC Mouse Anti-Human CD8 (BD Biosciences), PE-CY7 Mouse Anti-Human TNF-α (BD Biosciences), BV605 Mouse Anti-Human IFN-γ (BD Biosciences). After washed twice with stain buffer, cells were detected by BD FACS LSRFortessaTM instrument. Data was analyzed using FlowJo V10.

QUANTIFICATION AND STATISTICAL ANALYSIS

Data analyses were performed by GraphPad Prism 10 (GraphPad Software Inc., San Diego, CA) and R software. Unpaired two-tailed Student's t-tests were used to compare two groups. Differences among three or more groups were compared by Analysis of variance (ANOVA). The results are presented as mean ± standard deviation, and p value less than 0.05 was considered significant.